DEGREE PROGRAMME IN WIRELESS COMMUNICATIONS ENGINEERING

MASTER'S THESIS

DESIGN AND DEMOSTRATION OF DIGITAL PRE-DISTORTION USING SOFTWARE DEFINED RADIO

Author	Muhammad Hasibul Islam
Supervisor	Aarno Pärssinen
Second Examiner	Markku Juntti
Technical Advisor	Nuutti Tervo

March 2019

Islam Muhammad Hasibul (2019) Design and Demonstration of Digital Pre-distortion Using Software Defined Radio. University of Oulu, Degree Programme in Wireless Communications Engineering. Master's Thesis, 57 p.

ABSTRACT

High data rates for large number of users set tight requirements for signal quality measured in terms of error vector magnitude (EVM). In radio transmitters, nonlinear distortion dominated by power amplifiers (PAs) often limits the achievable EVM. However, the linearity can be improved by linearization techniques. Digital pre-distortion (DPD) is one of these widely used linearization techniques for an effective distortion reduction over a wide bandwidth. In DPD, the nonlinearity of the transmitter is pre-compensated in the digital domain to achieve linear output. Moreover, DPD is used to enable PAs to operate in the power-efficient region with a decent linearity.

As we are moving towards millimetre-wave frequencies to enable the wideband communications, the design of the DPD algorithm must be optimized in terms of performance and power consumption. Moreover, continuous development of wireless infrastructure motivates to make research on programmable and reconfigurable platforms in order to decrease the demonstration cost and time, especially for the demonstration purposes. This thesis illustrates and presents how software defined radio (SDR) platforms can be used to demonstrate DPD.

Universal software defined peripheral (USRP) X300 is a commercial software defined radio (SDR) platform. The chosen model, X300, has two independent channels equipped with individual transceiver cards. SIMULINK is used to communicate with the device and the two channels of X300 are used as transmitter and receiver simultaneously in full-duplex mode. Hence, a single USRP device is acting as an operational transmitter and feedback receiver, simultaneously. The implemented USRP design consists of SIMULINK based transceiver design and lookup table based DPD in which the coefficients are calculated in MATLAB offline. An external PA, i.e. ZFL-2000+ together with a directional coupler and attenuator are connected between the TX/RX port and RX2 port to measure the nonlinearity. The nonlinearity transceiver is measured with and without the external PA. The experimental results show decent performance for linearization by using the USRP platform. However, the results differ widely due to the used USRP transceiver parameterization and PA operational point. The 16 QAM test signal with 500 kHz bandwidth is fed to the USRP transmit chain. As an example, the DPD algorithm improves the EVM from 7.6% to 2.1% and also the ACPR is reduced around 10 dB with the 16 QAM input signal where approximately + 2.2 dBm input power applied to the external PA.

Key words: SDR, Transceiver, Digital Predistortion, Linearization.

Table of Contents

FOREWORD

I would like to convey my heartiest gratitude and profound respect to my supervisor professor Aarno Pärssinen for providing me the opportunity and guidance. Special thanks go to my technical adviser M.Sc. (Tech) Nuutti Tervo for his continuous guidance, suggestions and wholehearted supervision throughout the progress of this work. Without him, the thesis would have never been materialized. I am very grateful to him for acquainting me with the world of advanced telecommunication research.

I am grateful to professor Markku Juntti for providing me the opportunity and helpful comments. I would like to thank Dr. Shahriar Shahabuddin for mental support and help throughout the thesis. I want to acknowledge M.Sc. (Tech) Bilal Khan for fruitful discussions and suggestions. I would also like to thank the whole CWC staff for an excellent working environment.

I would like to thank my parents for their love, encouragement and inspiring me during my study period. Finally, I am grateful to the Almighty Allah for giving me the strength and patient to complete this Master's thesis.

Oulu, October, 05 2018
Muhammad Hasibul Islam

LIST OF ABBREVIATIONS AND SYMBOLS

ACI	Adjacent Channel Interference
ACP	Adjacent Channel Power
ACPR	Adjacent Channel Power Ratio
ADC	Analog to Digital Converter
ASIC	Application Specific Integrated Circuit
AM/AM	Amplitude to Amplitude Modulation
AM/PM	Amplitude to Phase Modulation
BER	Bit Error Rate
CIC	Cascaded Integrator Comb
DC	Direct Current
DAC	Digital to Analog Converter
DPD	Digital Pre-distortion
DDC	Digital Down Converter
DUC	Digital Up Converter
EVM	Error Vector Magnitude
FPGA	Field Programmable Gate Array
GPIB	General Purpose Interface BUS
GUI	Graphical User Interference
IF	Intermediate Frequency
IIP3	Third Order Intercept Point
IMD	Intermodulation Distortion
ISI	Inter-Symbol Interference
LNA	Low Noise Amplifier
LO	Local Oscillator
LPF	Low Pass Filter
LTE	Long Term Evolution
LS	Least Squares
LTI	Linear Time-Invariant
LUT	Lookup Table
MCM	Multicarrier Modulation
MP	Memory Polynomial
mm-Wave	Millimetre Wave
OFDM	Orthogonal Frequency Division Multiplexing
PA	Power Amplifier
PAPR	Peak to Average Power Ratio
PLL	Phase Locked Loop
PSD	Power Spectral Density
RRC	Root Raised Cosine
SCPI	Standard Commands for Programmable Instruments
SDR	Software Defined Radio

SMA	SubMiniature Version A
SNR	Signal to Noise Ratio
TF	Transfer Function
RF	Radio Frequency
QAM	Quadrature Amplitude Modulation
UHD	USRP Hardware Drive
USRP	Universal Software Radio Peripheral (Trademark of National Cooperation)
VCO	Voltage-controlled Oscillator

$ACPR$	Adjacent Channel Power Ratio
A_{e}	RMS amplitude Error Vector
A_{ref}	RMS amplitude of reference signal
α_p	Coefficient of p^{th} Order Nonlinearity
β	Roll-off factor
$\hat{d}_{\mathrm{km}}$	DPD Coefficient
$e(n)$	Estimation Error of n^{th} sample
$G(\lvert u(n)\rvert)$	Instantaneous Gain
K	Degree of PA Nonlinearity
M	Memory Depth
P	Order of Nonlinearity
P_{error}	Average Error Vector Power
P_{reff}	Average Ideal Reference Vector Power
$P_{\mathrm{t},ave}$	Average Transmit Power
P_{sat}	PA Saturation Power
$R(m)$	Cross Correlation between Input and Output
$S_{\mathrm{means},r}$	Normalized Constellation Point for r^{th} Measured Symbols
$S_{\mathrm{ideal},r}$	Ideal Normalized Constellation Point for r^{th} Symbols
t	Time Index
T	Symbol Period

1. INTRODUCTION

One of the challenges for the future wireless communication systems is to reduce the in-band distortion of a wireless transmitter to enable high spectral efficiency and high throughput. In addition, out-of-band emissions caused by the nonlinearity of the wireless transceiver induce unwanted interference to other users and systems, respectively. Traditionally, the wireless transmitter is designed in such a way that PA dominates the nonlinearity. The nonlinearity of a PA together with multicarrier modulation (MCM) signal having a high peak to average power ratio (PAPR) challenges for the future wireless communication system [1]. The next generation radios require better performance for faster application processing, i.e. baseband and also need power efficient RF devices to take care of wireless system physical signal transmission and reception. It also means higher demands of an adaptive algorithm to compensate the nonlinearity of the PA.

Figure 1 illustrates the traditional trade-off between the PA linearity and efficiency. The output power increases linearly as a function of input power but it is compressed after a certain point due to nonlinearity [5]. In general, efficiency and linearity of a PAs are inversely proportional to each other. In other words, the most efficient operation is often achieved in the nonlinear region. Moreover, utilization of high PAPR waveforms such as orthogonal frequency division multiplexing (OFDM) makes the problem worst. In the antenna input and finally at the over-the-air receiver, nonlinearity is seen as increased out-of-band emissions and decreased signal to distortion ratio. In-band distortion is usually described by using modulation error rate or EVM whereas out-of-band distortion is described in terms of the adjacent channel power ratio (ACPR).

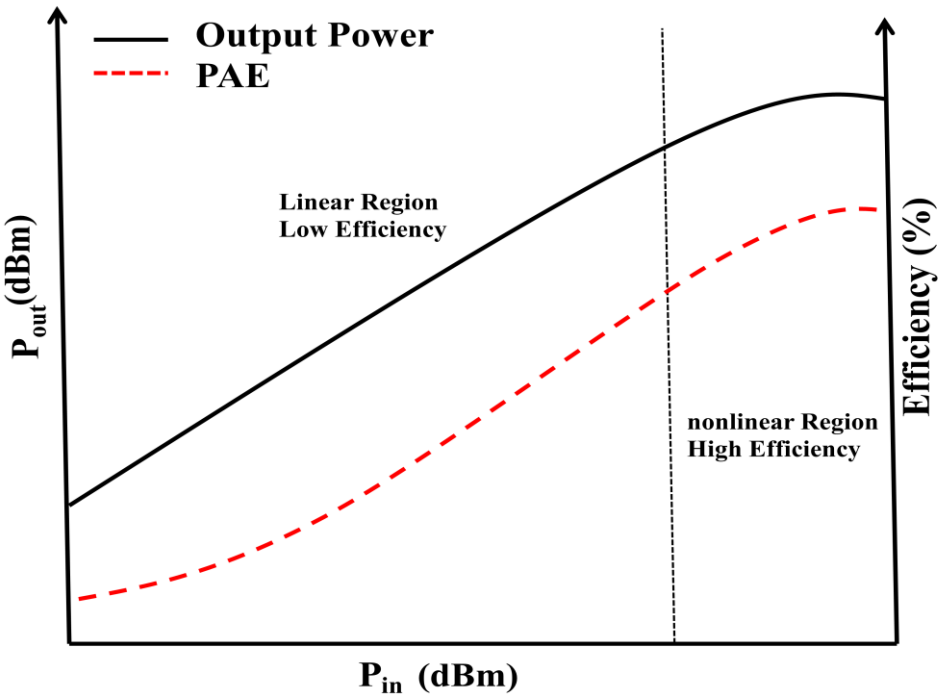

Figure 1. Trade-off between linearity and efficiency of PA.

In order to drive the PA in the nonlinear region with high PAPR waveform, different PA linearization techniques such as feedback, feed-forward and DPD linearization techniques are utilized in many practical systems. While feedback techniques suffer from instability problems, feed-forward carries its own analog delay [3]. Therefore, DPD techniques are often chosen due to its reconfigurable nature and better linearization purpose. DPD is a commonly used linearization technique in cellular base stations due to its effective interference reduction and relatively wide bandwidth. The core idea of the DPD is to pre-compensate the nonlinearity of the PA by applying the inverse function of the nonlinearity to the input in order to achieve linear output. To demonstrate the DPD algorithm, we chose commercial SDR platform, i.e. X300 USRP by National Instruments [44]. Here, the baseband part is presented in software, i.e. MATLAB and USRP operate as a RF and digital front end. This combination of the software and hardware helps to achieve rapid design and demonstration of the algorithm as a part of a digital communication system.

The thesis is organized as follows. In chapter 2, the behaviour model of the PA and also different RF impairments of the PA nonlinearity is discussed briefly. The linearization techniques with the delay alignment and power normalization process also described. Chapter 3 represents the basic signal transmission process in the SDR platform, i.e. USRP X300 using MATLAB interface. The chapter 3 also discusses the behaviour of the demonstration platform and also shows the inherent nonlinearity of the platform itself, i.e. CBX daughterboard of the USRP. The demonstration of the DPD algorithm is discussed in chapter 4. The DPD performance is analyzed based on the experimental results. Finally, chapter 5 discuss about the effects of transceiver nonlinearity in the SDR platform and also presents possible future work.

2. POWER AMPLIFIER NONLINEARITY AND LINEARIZATION

The PAs are often driven in the nonlinear region to achieve better efficiency with high PAPR. As a result, the nonlinearity causes phase as well as amplitude distortion. The linearization technique helps to recover the back-off by operating the PA close to the compression region with a decent linearity. The linearity of a practical system depends on the order of nonlinearity. So, the optimum approach should be proper PA behaviour modelling and also perfectly characterization of the PA nonlinearities for linearization. In this chapter, parameters to characterize PA nonlinearities and mathematical model for the linearization are presented.

2.1. Nonlinearity of Power Amplifier

In the RF transmitter, the purpose of PA is to produce the required transmit power to the antenna input with good efficiency. High power makes PA traditionally as the most power-hungry component of a wireless transmitter. When operating in high power region, few per cent efficiencies means that most of the power consumed by the transceiver is turned into heat which has to be conducted to the heat sink and cooled down by fans and large area. Hence, PA has usually the dominant role in the whole transceiver efficiency and power consumption. Figure 2 presents the traditional PA output power behaviour as a function of input power. When the PA input power is increased towards the saturation power, the output of the PA is compressed. The point where the output power differs 1 dB with respect to a linear value is known as 1 dB compression point [61].

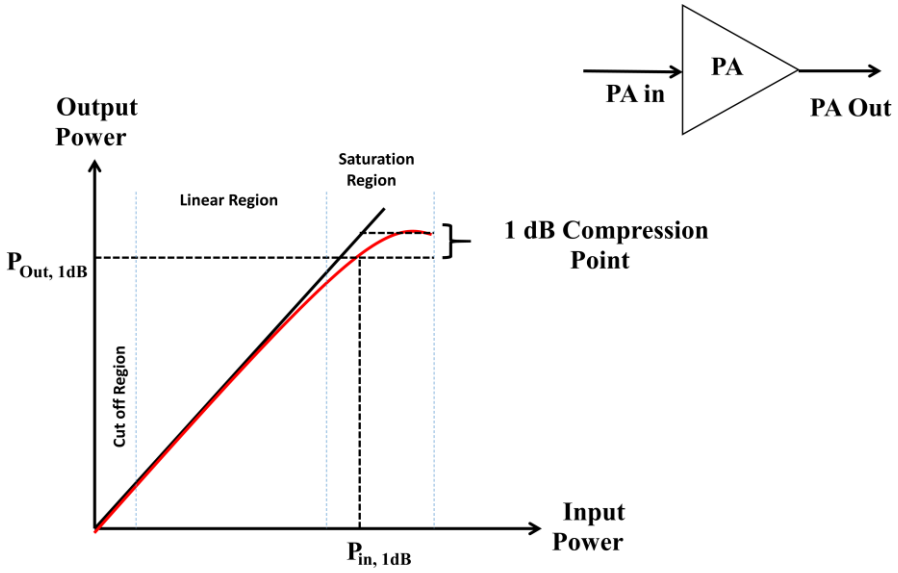

Figure 2. Power amplifier nonlinearity.

2.1.1. AM/AM and AM/PM Distortion

In the baseband side, transmit data is encoded in amplitude and phase. In order to operate PA in efficient region, we increased the input amplitude of the PA as a result the output power became saturated, which means PA operates in the nonlinear region. Actually, the output signal is compressed since it does not have now the linear gain. In this thesis, the amplitude to amplitude conversion (AM/AM) and amplitude to phase conversion (AM/PM) are characterized by using modulated signals even though traditionally single-tone test is used. AM/AM distortion describes the compression of the signal envelope as a function of the input signal amplitude. After that, the amplification may not take place over the whole signal cycle. In an ideal case, PA gain has constant phase over signal dynamic range. In a practical case, the phase of the gain changes with the input amplitude known as AM/PM distortion. Here, the resulting phase angle delay will be the difference between the fundamental frequency and the harmonic, during that time there are no phase change between the input and output signal at the fundamental frequency. The time delay increases with a frequency within the bandwidth of PA and also depends on the PA design [5].

2.1.2. Intermodulation Distortion

Under the large signal condition, the PA operates in the nonlinear region which causes distortion in the output. The deviation from the linearity occurs additional frequencies components in the output signal known as intermodulation distortion (IMD). It is a cross product of two or more fundamental signals causing several unwanted frequency components to the output. Traditionally, the IMD is measured by the two-tone test. It is the standard way to characterize the nonlinearity. With the modulated wideband signal, similar IMD products can be seen as increased adjacent channel power.

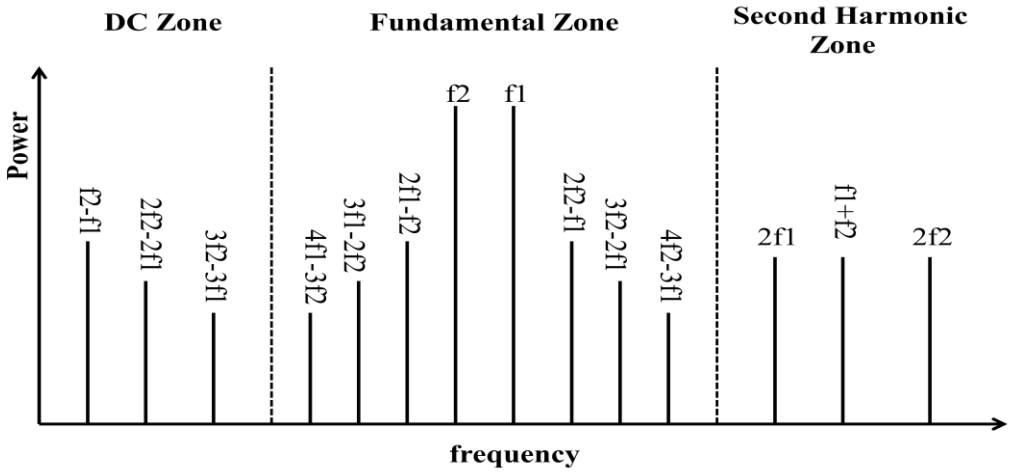

Figure 3. Harmonics and IMD products for two-tone input.

Figure 3 presents the harmonics and IMD products for a two-tone input signal. As it can be noticed from the figure, the second order intermodulation and harmonic distortion occur at frequencies f_1+f_2 and f_1-f_2, those filtered away in the transmitter. Odd order such as third order nonlinearity causes IMD which occurs at frequencies $2f_1-f_2$ and $2f_2-f_1$ close to the signal band causes distortion to the desired signal. Third order IMD is proportional to the cube of the input signal and second order IMD is proportional to the square of the input signal [6]. Third, fifth and higher order IMD products are responsible for the distortion of the output power which cannot be fully removed by analog filtering from the PA output. Here, figure 4 shows the intercept and 1 dB compression points. As seen in figure 4, the increased slope of output power and third order intermodulation product intersects at a certain point known as third-order intercept point which is impossible to achieve since output powers are saturated below this level. If we decrease the input power by 1 dB than all third order products level is decreased by 3 dB [7]. Thus, the intercept point is an important figure of merit to evaluate the distortion level of PA at a given operating point.

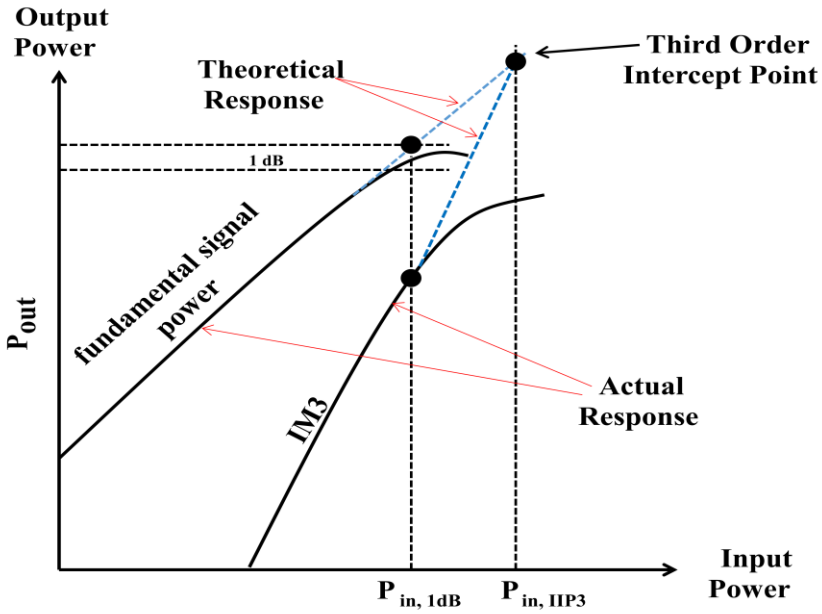

Figure 4. Intercept and 1 dB compression point.

2.1.3. Spectral Regrowth and ACPR

Modulated signals are suffering from the spectral regrowth at a given input power of the PA. Spectral regrowth is a nonlinear phenomenon that can be observed in the frequency domain. Due to the mixing products between the individual frequency components, the spectral content observed at the PA output becomes broader by the odd order nonlinearities which increase the adjacent channel interference (ACI) [8]. The leakage in the adjacent channel power (ACP) mainly occurs due to IMD products.

The IMD results to an adjacent channel power ratio (ACPR) which is the ratio between the main channel power and total power integrated over the adjacent channel band. In other words, the power ratio between the adjacent channel and the reference channel is known as ACPR. We can calculate ACPR for both adjacent channels as,

$$\mathrm{ACPR} = 10\log\left|\frac{\int_{\mathrm{main}} S(f)df}{\int_{\mathrm{adjleft}} S(f)df + \int_{\mathrm{adjright}} S(f)df}\right| \quad (1)$$

where $S(f)$ is the power spectral density (PSD) of the output power and the term adj represents either the upper channel or the lower channel [9]. Figure 5 shows the spectral regrowth at a given input power. The upper ACPR is the power from the assigned channel which is leaked into the channel above. And lower ACPR is the power from the assigned channel which is leaked into the channel below [56,59]. As we can see from the figure, a small transition band between the main channel and adjacent channel are reserved in order to reduce the inter symbol interference (ISI). This is because of roll off of the pulse shaping filter. Note that, roll-off factor (β) is responsible for specifying the bandwidth (β/2T), where T is the symbol period.

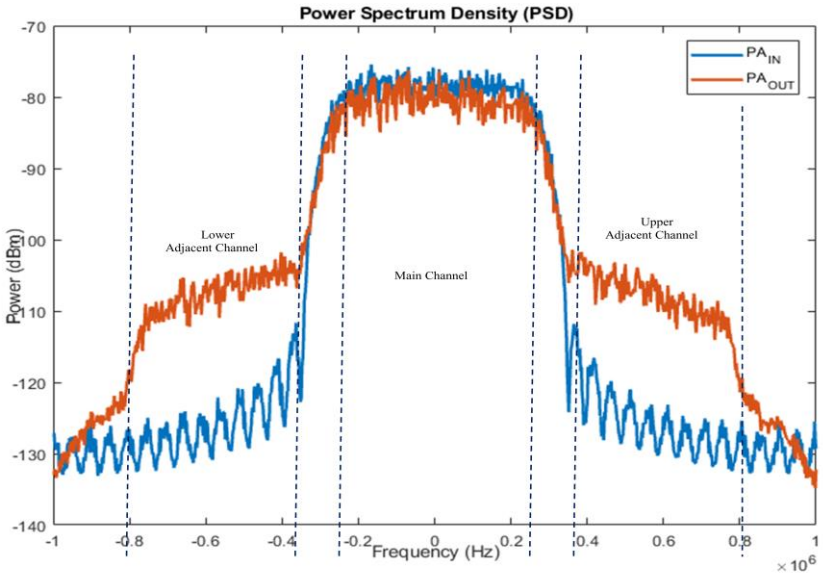

Figure 5. Spectrum regrowth.

2.1.4. Error Vector Magnitude

In a practical system, it is important to know the in-band performance of a transmitter or receiver which can be evaluated by the EVM. Increasing the modulation order tightens the EVM requirement for a fixed bit error rate (BER) specification. In order to obtain better power efficiency, the PA should be operated as close as possible to the saturation region which creates a distorted output signal due to the nonlinearity. This nonlinear distortion produces in-band interference that occurs in the deviation of phase and amplitude of the modulated vector signal. EVM is a figure of merit for modulation accuracy that illustrates the phase and amplitude distortions as well as noise and quality of the system. Figure 6 presents the EVM between the reference symbol vectors and measured symbol vector. If we notice the measured symbol which is not in the actual position, the phase and magnitude are shifted from their reference point. The angle between the reference symbol vectors and measured symbol vectors known as a phase error. The difference between the reference symbols and the measured symbols known as EVM [10]. And the increased magnitude concerning reference symbol vectors called as magnitude error.

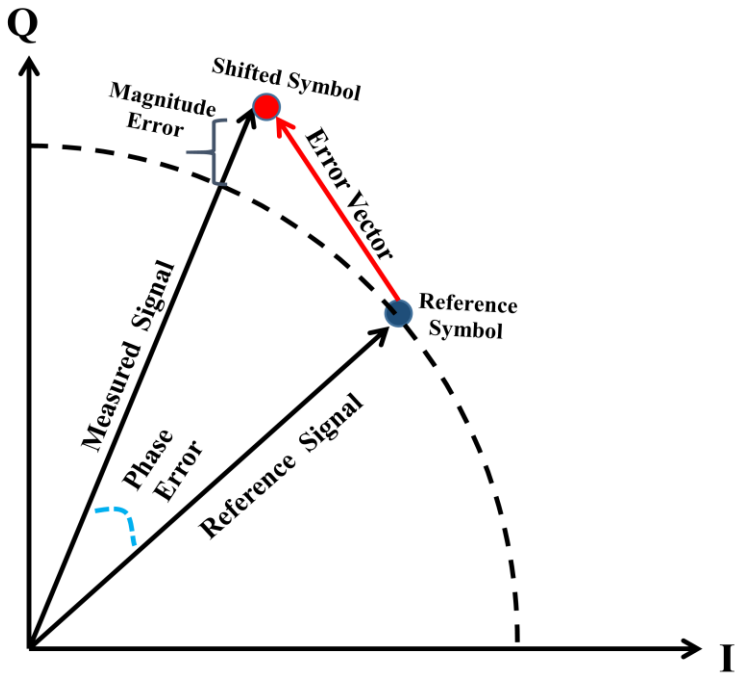

Figure 6. Error vector magnitude.

The EVM is characterized as RMS value [11] as

$$\mathrm{EVM_{RMS}} = \left| \frac{\frac{1}{N}\sum_{r=1}^{N} \left| S_{\mathrm{ideal},r} - S_{\mathrm{means},r} \right|^2}{\frac{1}{N}\sum_{r=1}^{N} \left| S_{\mathrm{ideal},r} \right|^2} \right|^2 \tag{2}$$

where N is the number of constellation points, $S_{\mathrm{means},r}$ is the normalized constellation point for the r^{th} measured symbol and $S_{\mathrm{ideal},r}$ is the ideal normalized constellation point for the r^{th} symbol.

2.1.5. Memory Effect

Memory effect of the PA means that the output is not only dependent on the current input sample, but also previous input samples [5]. The PA output depends on the previous input value due to the delay caused by the thermal and electrical effects in the PA circuitry [13]. If the PA is considered as memoryless then third order intermodulation only depends on the input amplitude, but in reality it also depends on the spacing of different tone. Now, we can say that any non-constant distortion behaviour at different tone spacing is called memory effect [14].

Memory means that the device remembers the value of a signal for a certain time. In the frequency domain, this means the frequency response is not flat. Nonlinear device can have linear and nonlinear memory in the input side and output side and even also in the feedback such as Wiener, Hammerstein, Wiener-Hammerstein model which has memory dependent coupling from PA output to input. The non-ideal fundamental frequency response is caused by the linear memory effect whereas the nonlinear memory effect depends on the trapping effects, impedance matching and also bias circuit design [15, 45].

There are two types of memory effects, electrothermal memory effects and electrical memory effects. The main reason for electrical memory is impedance variation at DC, fundamental and harmonic bands at the envelope frequency or different modulation frequencies [16]. The variations of the impedance occur from the bias network of the transistors which generates unwanted signals with the same frequencies as an IMD product [17, 60]. The voltage waveforms of the different nodes at the envelope frequency are affected by node impedances. The transistor changes its properties at different temperature due to the electrothermal memory effects. The power dissipation of the PA is determined by the thermal impedance of the transistors. It occurs due to the temperature change with respect to the frequency which acts as a low pass filter. The thermal temperature changes on the envelope frequency might effect on gain, capacitance and output conductance of the PA [14].

2.1.6. Power Back-off

In the transceiver, back-off is required in order to allow a varying envelope waveform to have a full signal swing at the output. In general, back-off is defined as a back off of current operation point from the saturation or a compression point, depending on the definition. For linear operation, back off should be more than the PAPR of the waveform. In the back-off mode, we simply reduce the input power of the PA such that PA becomes more linear. This means that the maximum input power level of the PA must be restricted such as the output signal stays close to the weakly nonlinear region. Back-off reduces the output power level of the PA typically 6-8 dB to improve the PA linearity. However, there is a trade-off between power efficiency and linearity. While the back-off of the PA is decreased, the efficiency level will increase. In the digital modulation, we expected that the back-off is around 6 dB from the 1 dB compression point [16]. The PA output back-off (OBO) can be defined as

$$\mathrm{OBO} = -10 \log_{10} \frac{P_{\mathrm{t,ave}}}{P_{\mathrm{sat}}} \tag{3}$$

where $P_{\mathrm{t,ave}}$ is the average transmit power and P_{sat} is the PA saturation point. Moreover, the back-off depends on the crest factor of the modulated signal which means the PAPR of the modulated signal. The back-off can be mitigated by reducing the PAPR of the baseband signal through clipping, filtering and crest factor reduction (CFR).

2.2. Behavioural Modelling of Nonlinearity

The mathematical model of the input-to-output relation of a certain device can be represented by a behavioural model [7]. In this case, the system level behaviour of a PA can be modelled as a "black box". For example, we have no knowledge of the internal structure and characteristic of a device for the output responses, but we can still characterize its input-output relation by measurement based model. Therefore, we can estimate the behaviour of the parameters by observing the measured output. In such a way, we can mathematically model the nonlinearity and memory effects of the PAs. Pre-distortion model for PA is crucial in order to predict the nonlinearity of the PA. The behaviour of the PA is modelled as a black box and the inverse function of this block box function would be the pre-distortion model. The behaviour models of the PA can be roughly classified as a memoryless model, a model with linear memory and models with nonlinear memory [57]. Simplified memoryless nonlinearity of a PA can be modelled as a Taylor polynomial as

$$V_{\mathrm{out}}(t) = \alpha_1 V_{\mathrm{in}}(t) + \alpha_2 V_{\mathrm{in}}^2(t) + \alpha_3 V_{\mathrm{in}}^3(t) + \cdots + \alpha_p V_{\mathrm{in}}^p(t) \tag{4}$$

where, $V_{\mathrm{out}}(t)$ is the output signal, $V_{\mathrm{in}}(t)$ is the input signal with different time index t and α_1 is the linear gain coefficient and $\alpha_2, \alpha_3, \alpha_4, \ldots\ldots, \alpha_{\mathrm{p}}$ are the coefficients for different order of nonlinearity. Even order IMD products do not affect on a fundamental signal. However, odd order intermodulation distortion (IMD) products induce the gain compression as a result output signals are distorted [19].

2.2.1. Memoryless Models

When the instantaneous output of the PA only depends on the instantaneous input, the model is considered to be memoryless. The memoryless model can be characterized by the AM/AM and AM/PM of a particular PA which represents the output power or amplitude and phase as a function of input power or amplitude. In this method, raw measurement data are used to fit a complex-valued polynomial to model AM/AM and AM/PM distortion. In the memoryless model, the AM/AM distortion function tries to model the saturated output power due to the gain compression. And AM/PM distortion function tries to model the phase dependency of the output as a function of input amplitude [20]. If coefficients of the memoryless model are real values, AM/PM conversion is zero. On the other hand, the complex coefficient of the memoryless model yielding nonzero AM/PM distortion indicating the quasi-memoryless nonlinearity [21]. The memoryless model defined as

$$y_{\text{out}}(n) = \sum_{p=1}^{P} a_p x^p(n) \tag{5}$$

where $y_{\text{out}}(n)$ is the output signal, $x^p(n)$ is the input signal with different order of the polynomial function denotes as p, and the coefficient a_p determine the distortion of the PA.

2.2.2. Nonlinear Models with Linear Memory

The memoryless PA model [54,15] deals with the frequency independent cases where the input signal bandwidth is much less than the bandwidth of the amplifier. Hence, the frequency response of the memoryless PA model is flat. However, PA exhibits the frequency dependent behaviour which can be considered as a frequency selective channel. The output signal of the PA depends on the previous input values due to delay induces by the thermal and electrical memory effects in the PA circuitry. In the test bench, the frequency dependent PA model or memory based nonlinear model will be verified. In the previous section, the quasi memoryless model as introduced where the short term memory is used to describe the phase distortion by the complex nonlinear coefficient. In this section, we will illustrate the memory based nonlinear models in the literature to characterise the PA nonlinearity. Nonlinear models with linear memory are models that consist of an input filter that is cascaded with a memoryless nonlinearity or vice versa for a nonlinear PA or pre-distortion. Figure 7(a) presents two box model consider as Wiener model that comprised of a linear filter followed by a memoryless static nonlinearity.

$$y(n) = \sum_{p=1}^{P} a_p \left[\sum_{m=0}^{M} h_m u(n-m)\right] \sum_{m=0}^{M} |h_m\, u(n-m)|^{p-1} \tag{6}$$

where P is the nonlinear order and M is the memory depth, $u(n)$ intermediate signals and h_m and a_p are the model parameters.

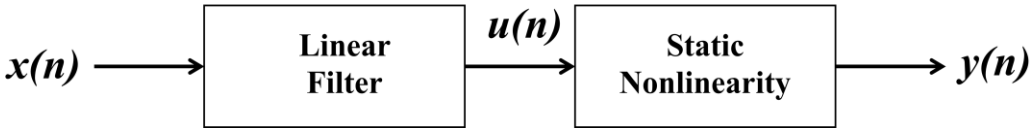

(a) Weiner Model.

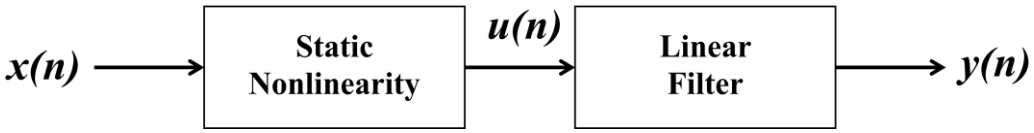

(b) Hammerstein Model.

Figure 7. Nonlinear model with linear memory.

Figure 7(b) presents two box model called as Hammerstein model that consists of a static nonlinearity followed by a linear filter or linear time-invariant (LTI) system. In this two-box model input filter is cascaded with a memoryless nonlinearity or vice versa for a nonlinear PA or pre-distortion. Here, the static nonlinearity box characterises the AM/AM and AM/PM distortion and the filter box consider as a frequency response of the nonlinear device [22, 53]. The complex Hammerstein model is given by

$$y(n) = \sum_{m=0}^{M} h_m \left[\sum_{p=1}^{P} a_p u(n-m)|u(n-m)|^{p-1} \right] \tag{7}$$

2.2.3. Nonlinear Models with Nonlinear Memory

Accurate behavioural models are necessary for the nonlinear memory effects. The Volterra model has been used extensively to model the nonlinearity of the PA which includes the memory effects. The complexity to determine the model parameters is quite high and consists of large number of parameters. Therefore, a simplified Volterra based model is known memory polynomial (MP) model [41, 15]. The polynomial (MP) model form for the PA can be formulated as

$$y_{\mathrm{MP}}(n) = \sum_{k=0}^{K-1} \sum_{m=0}^{M-1} a_{km} x(n-m)|x(n-m)|^{k} \tag{8}$$

where a_{km} are the PA polynomial coefficients, n is the time index, M is the memory depth and K is the degree of the PA nonlinearity. The linearization performance depends on the methods used to calculate the coefficient. However, it will also add computational complexity if the number of the parameter such as memory depth and the degree of the PA increase exponentially.

2.3. Linearization Techniques

The aim of any linearization technique is to compensate the nonlinearity by shaping the input or output waveform of the PA. The linearization can be categorized into circuit level and system level techniques, respectively. Circuit-level techniques are for example harmonic termination and injection, transconductance gain compensation for field effect transistor (FET) amplifier, active biasing for dynamic power supply. It reduces the power consumption and finally the thermal compensation approaches. The circuit-level linearization techniques are very suitable especially for user terminal equipment due to their low power consumption. On the other hand, system-level approaches are roughly divided into digital and analog techniques. Some analog techniques are feed-forward, feedback, analog pre-distortion, envelope elimination, and also restoration and linear amplification with nonlinear components (LINC) [26]. Also, digital implementations of the system level techniques often require a significant amount of DSP power which is not available in a battery operated the device. Moreover, circuit level linearization can be used together with system level techniques. The system-level approaches are suitable for the base station transmitters due to the high amount of available processing capacity for DSP and high power consumption of PA. In this section, we focused mainly on the system level linearization.

2.3.1. Feedback Linearization

In the feedback linearization, a feedback loop is used to sample the PA output in order to separate the nonlinear content from it and add a scaled and phase inverted version of it to the input. This is done in order to pre-compensate the linearity to achieve linear output. The principle of this operation is to separate the error signal from the output by comparing the input signal. After that, the output signal is fed back to the input of the PA with opposite phase [27]. Figure 8 shows a feedback linearization technique where a comparator is used to calculate the error signal $V_e(t)$ from the input signal $V_i(t)$ and the signal $V_r(t)$ from the feedback path. After that, the error signal is fed to the PA to achieve a linear output.

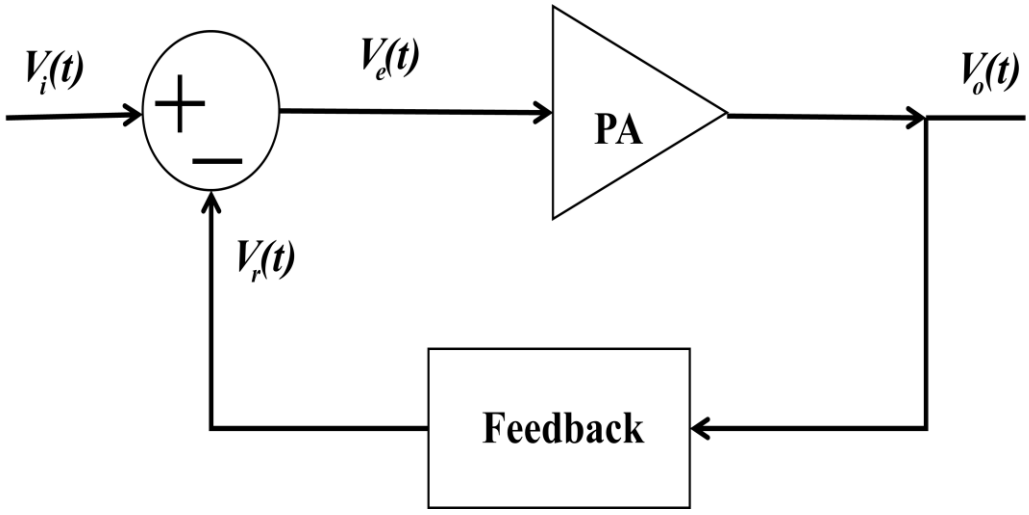

Figure 8. Feedback linearization [27].

The delay between the input and output signal makes feedback linearization very sensitive for stability problems. Several methods of the feedback linearization techniques are used as linear the output such as Cartesian feedback and envelope feedback. In Cartesian feedback, the linearization uses a separate loop for in-phase (I) and quadrature (Q) components. Hence, the error is computed separately for the in-phase and quadrature components. The slow variation of the input signal mitigates the delay between the input and output to increase the stability. In envelope feedback linearization [50], the envelope of the signal is detected and modified. Figure 9 presents a block chart of the envelope feedback linearization system. The comparison of the generated signal and envelope detector fed to gain controller through a low pass filter to remove the nonlinearity of the PA.

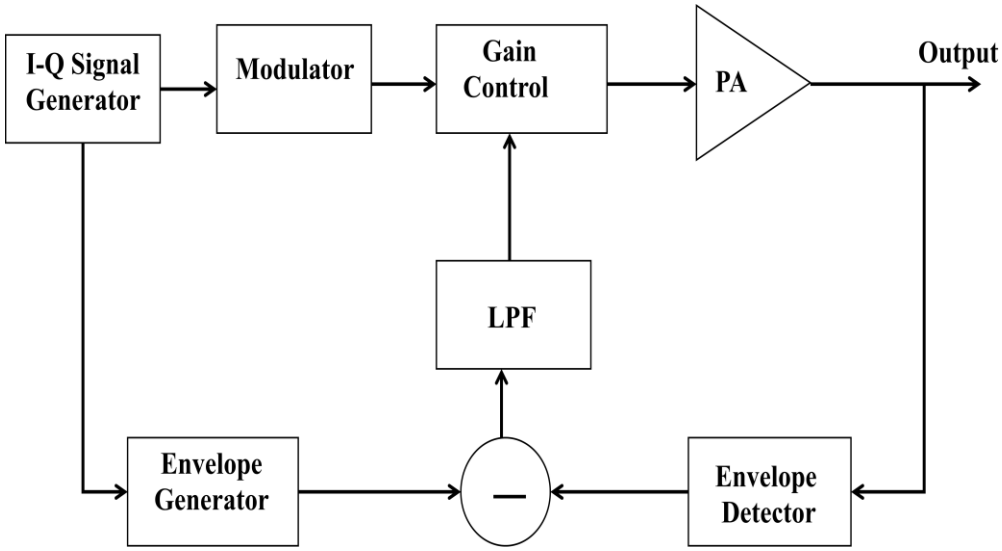

Figure 9. Envelope feedback linearization [50].

2.3.2. Feedforward Linearization

In the feedforward linearization, the distorted output is post compensated by adding a phase inverted version of the nonlinear content to the PA output. The block diagram of the feedforward linearization technique given in Figure 10. In this technique, the input is divided into signal cancellation and error cancellation loops. The distortion caused by the PA is estimated by the signal cancellation loop. At first, the input signal is separated by the directional coupler C_1 into two paths where the first one fed to the PA and the second one enters to delay circuit. The attenuator L_C and the delay circuit ensure that the signal should be synchronized and same power level in the directional coupler C_3 which yields to error signal $e(t)$ of the PA. Finally, the error signal $e(t)$ and the output signal are fed to the error cancellation loop to remove the distortion. However, the error signal $e(t)$ passes through the attenuator to scale and tune the phase before amplification to the desired power level. In the end, upper and lower branch signals are fed to the directional coupler C_4 in order to remove the error signal and generate the distortionless signal $z(t)$ [15].

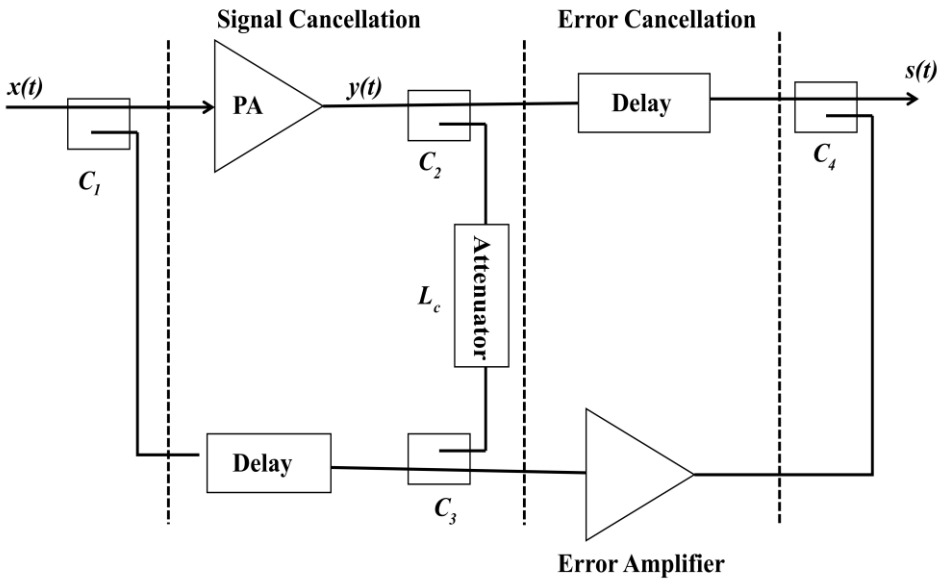

Figure 10. Feedforward linearization [15].

2.3.3. Digital Pre-distortion

In digital pre-distortion, the input signal is directly fed through a block called the pre-distorter which is a nonlinear system to counteract with the PA's nonlinearity. The pre-distorter block works as an inverse function of the PA is cascaded with the PA to make the output of the two blocks linear [58]. Figure 11 shows the basic principle of DPD linearization system. In the figure, we illustrate the DPD linearization system in the frequency domain where input signal $x(n)$ feds to the pre-distorter to induce $u(n)$ in order to make linear PA output $y(n)$.

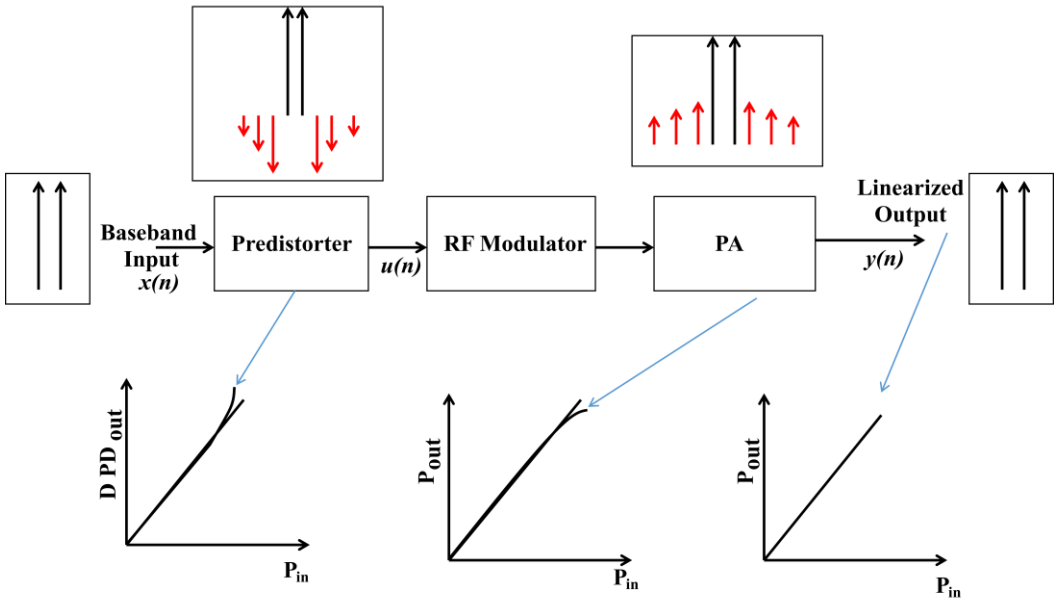

Figure 11. Digital pre-distortion linearization system.

The major challenge in the DPD linearization is to find the inverse function of a nonlinear system. The PA characteristics are changed for temperature variations, power supply voltage and also for aging. In general, DPD should be updated constantly as the power, temperature, together with several other environmental conditions are changing over time. The DPD model is usually valid over the time the environment and operation parameters such as power remains constant. However, periodical tracking of the dynamic PA behaviour and adapting the pre-distortion function requires real time processing was not possible in this thesis with SIMULINK based control software.

Moreover, DPD cannot as such remove the back-off totally, but it enables the PA to operate closer to the compression (smaller back-off) with good linearity. Therefore, back-off is still required even DPD was used in order to enable decent signal swing at the output. So all in all, DPD does not avoid the back-off totally, we still need CFR in order to have the varying envelope in the PA output. But, DPD can linearize the PA in back-off conditions close to the PAPR of the waveform.

2.3.3.1. Static DPD Implementation

In general, the DPD should be designed to be adaptive for varying operation conditions. However, for the demonstration purpose, we can fix the conditions to the chosen ones such that the nonlinearity becomes more static. Static DPD cannot follow the changes in the data but if the static DPD coefficients are calculated over long enough set of samples, the average results are sufficient for the demonstration purpose. Static DPD can be implemented as a look-up-table (LUT). LUT is a table in the memory which contains the static pre-distortion coefficients to a certain operation point. LUT is valid only to the operation point to which it is trained. There are also many approaches, for example, one may have multidimensional LUT where the coefficients are trained for different operation points.

For static DPD, often the simple model is better because it is more stable. If you have the high number of coefficients, the rarest ones are usually the ones which change with the environment etc. However, with less coefficients they have less meaning, although performance can be reduced compared with the more complex models. The adaptive pre-distortion uses feedback techniques to make a robust solution due to the random change of the PA characteristics. Even in the LUT approach, the parameters and the coefficient can be determined by the adaptive algorithm, i.e. the least square (LS) method. There are two different adaptive DPD architectures; one is direct learning architecture and other is indirect learning architecture.

2.3.3.2. Direct Learning Architecture

In the direct learning architecture [51], the PA characteristics are initially defined, then the inverse of the PA model is computed by a static or iterative method. This architecture is applicable for the memoryless PA whereas the PA function inversion might be complicated for the memory dependent PA model. The difference between the input and normalized output is the error signal which is used to update the coefficients of the pre-distorter. The complexity of the model derivation comes from the number of coefficients. In general, more coefficients mean that more data is required for training, i.e. to fit the polynomial to the available data. Figure 12 shows the direct learning architecture where the input signal $x[n]$ is fed to the pre-distorter block then the pre-distorted signal $z[n]$ drive the PA. The difference between the input and the output from the PA is error signal $e[n]$. Finally, the parameters of the pre-distorter are updated by minimizing the error signal.

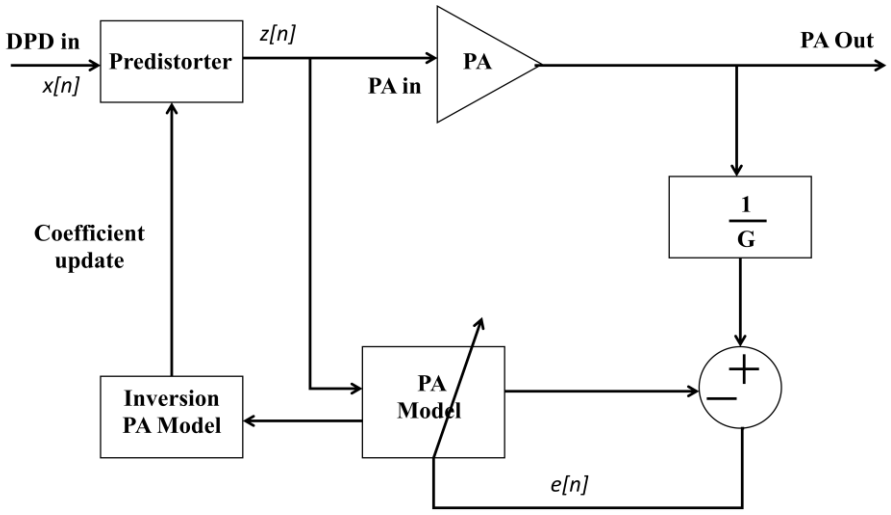

Figure 12. Direct learning architecture [51].

2.3.3.3. Indirect Learning Architecture

In the indirect learning architecture, the post-inverse of the PA is first identified by interchanging the input and output signals. Hence, in indirect learning the system does not learn the PA behaviour but it models directly the inverse of it. However, this architecture suffers from low input power when the linearity is already high, i.e. under large back-off range due to the interchanging of the input and output signal during calculation of the post-inverse. Hence, the limits for the operation of the PA up to a particular input power level which is far below the saturation point [15]. Figure 13 shows the direct learning architecture where the input signal $x[n]$ is fed to the pre-distorter then the pre-distorted signal $z[n]$ drive the PA. Next, the normalized output from the PA $y[n]$ is fed to the pre-distorter model, resulting in pre-distorter model estimates $\hat{z}[n]$. The difference between the pre-distorter model estimate $\hat{z}[n]$ and the pre-distorted signal $z[n]$ is the error signal. Finally, the parameters of the pre-distorter are updated by minimizing the error signal [17].

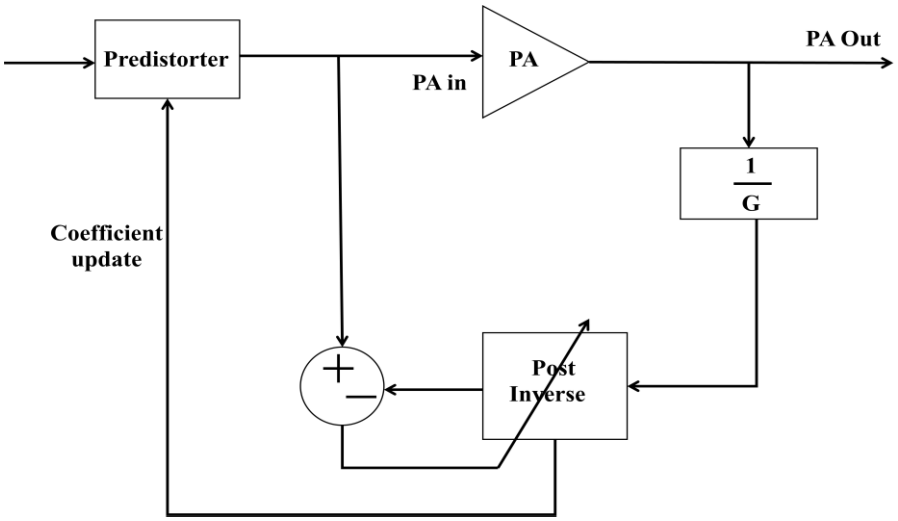

Figure 13. Indirect learning architecture.

2.3.3.4. Closed Loop Adaptive Digital Pre-distortion

In figure 14, a block chart of adaptive closed loop DPD architecture is shown. In this architecture, the pre-distorter is inside of the feedback adaptation loop which is used to update the pre-distorter parameters. Adaptive algorithm is used to update the pre-distorter parameters where the error signal is calculated by the input and output signals of the PA. In this system, the convergence is achieved in the subsequent loop by minimising the distortion signal. When compared with the direct and indirect learning architecture, the closed loop estimation is less sensitive to noisy feedback observation [15, 52].

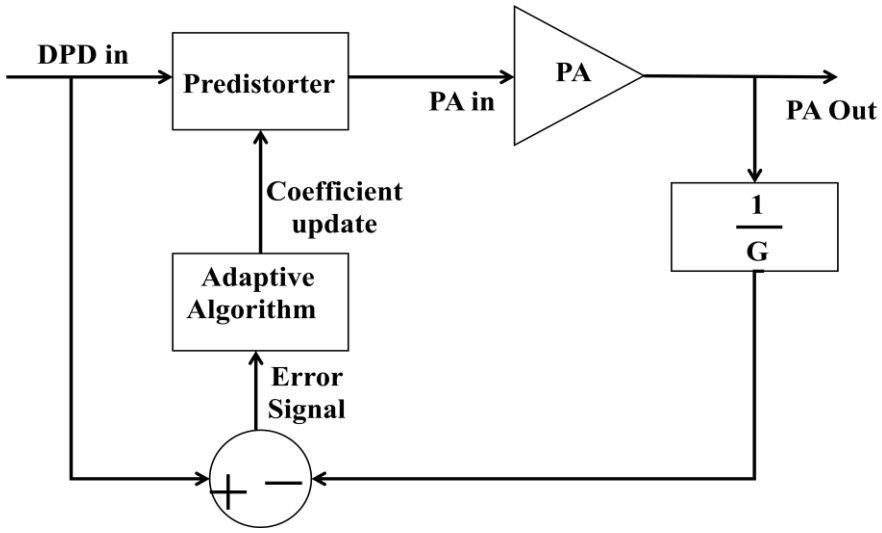

Figure 14. Closed loop adaptive digital pre-distortion.

2.4. Coefficient Extraction for Static DPD

There are a number of estimation algorithms for estimating the model coefficients that apply a linear weighting of the nonlinear signals such as the coefficient of the memory polynomial pre-distorter presented in equation (13). Figure 15 illustrates the graphical presentation of coefficient derivation and demonstration process [23]. The top path represents the PA behaviour model in which the nonlinearity of the PA is presented by the nonlinear function $f(x_1, x_2, \dots, x_n)$ and linear gain G.

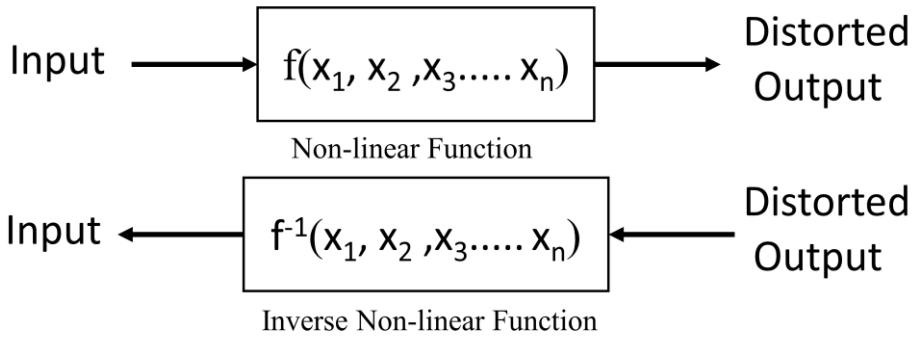

Figure 15. Block diagram for coefficient derivation.

The mathematical representation of a memory polynomial (MP) of the PA nonlinear function $f(x_1, x_2, \dots, x_n)$ can be formulated as

$$y_{\mathrm{MP}}(n) = \sum_{k=0}^{K-1} \sum_{m=0}^{M-1} a_{\mathrm{km}} x(n-m)|x(n-m)|^k \tag{9}$$

where, y_{MP} is a memory polynomial of the PA output, a_{km} are the PA polynomial coefficients, n is the time index, M is the memory depth and K is the degree of the PA nonlinearity. The input samples $x(n)$ are collected in a column vector $N \times 1$, where N is a total number of signal samples. The PA polynomial coefficients a_{km} are collected in a column vector $j \times 1$, where j is a number of polynomial coefficients. And the input samples $x(n)$ are collected in a column vector $N \times 1$ are organise the input sample vector in such a way that each PA polynomial coefficients d_{km} is associated with the input samples $x(n)$ as in equation (12). For example, the PA polynomial coefficients d_{31} is associated with $x(n-m)|x(n-m)|^2$, where the degree of the PA nonlinearity k = 3 and memory depth m = 1 respectively [24].

$$X_{\mathrm{km}}(n) = x(n-m)|x(n-m)|^{k-1} \tag{10}$$

Now, X_{km} is assembling into $N \times \mathrm{j}$ matrix. The process for generating the inverse of the MP model is represented at the bottom of figure 15. The process is divided into a inverse non-linear function $f^{-1}(x_1, x_2, \dots, x_n)$ multiplied with the inverse of the linear gain $\frac{1}{G}$. The mathematical expression of the inverse nonlinear function fitted to the measured output data $f^{-1}(x_1, x_2, \dots, x_n)$ can be written as

$$x_{\mathrm{MP}}(n) = \sum_{k=0}^{K-1} \sum_{m=0}^{M-1} d_{\mathrm{km}} y(n-m)|y(n-m)|^k \tag{11}$$

where $y(n)$ is the n^{th} measured sample in the PA output. In order to solve the PA polynomial coefficients d_{km} are collected in a column vector $j \times 1$, where j is the total number of coefficient represents the equation (18) as a linear equation

$$\begin{bmatrix} x_n \\ x_{n+1} \\ \vdots \\ x_{n+p} \end{bmatrix} = \begin{bmatrix} y(n) & y(n-1) & \cdots & y(n-M+1)|y(n-M+1)|^{K-1} \\ y(n+1) & y(n+1-1) & \vdots & y(n-M+2)|y(n-M+2)|^{K-1} \\ \vdots & \vdots & & \vdots \\ y(n+p) & y(n-1+p) & \cdots & y(n-M+1+p)|y(n-M+1+p)|^{K-1} \end{bmatrix} \begin{bmatrix} d_{00} \\ d_{01} \\ \vdots \\ d_{\mathrm{K-1,M-1}} \end{bmatrix}$$

$$\hat{x} = Yd \tag{12}$$

where p denotes the number of measurement samples which is typically greater than the products of $K \times M$. Now, the input samples are being estimated from the output samples Y of the PA which multiply with the PA polynomial coefficients d. The estimation error $e(n)$ is written as $e(n) = x(n) - \hat{x}(n)$. After assembling the observation matrix with known input and output samples, the polynomial coefficients $\hat{d}_{\mathrm{km}}$ of the inverse PA model can be formulated by the least square (LS) solution as

$$\hat{d}_{\mathrm{km}} = (Y^H Y)^{-1} Y^H X \tag{13}$$

where, Y^H is the conjugate transpose of the matrix Y. This PA polynomial coefficients derivation process is applied over samples which decrease the storage requirements [25]. The LS solution consumed some memory due to increased amount of samples. In general, LS solution in closed form is not practical for DPD since it requires calculation of a inverse for relatively large matrix. Usually, iterative adaptive algorithms are used to approximate the least squares solution in practice. However, for our purpose, simple static LS solution provides decent performance in order to make demonstration about the DPD process.

2.5. Delay Alignment and Power Normalization

In the pre-distortion scheme, the delay between the input and output exist because of the analog and digital circuitries and physical distance between the transmitter and observation receiver. The modelling approaches of the pre-distorter are based on the input and output signal. Hence, proper synchronization is required to align the input and output samples correctly for the comparison. If the delay between the waveform is not compensated, the modelling becomes inaccurate due to the delay induces dispersion in the AM/AM and AM/PM characteristics of the PA. In our demonstration, the simple correlation-based method is used for delay alignment. The cross-correlation between the input and output can be calculated as

$$\mathrm{R}(n) = \sum_{n=0}^{N-1} z(n)\, z_{\mathrm{pa}}^{*}(n+m) \tag{14}$$

where z and z_{pa} are the input and output, N is the length of the sequences, m is the delay variable and the correlation $R(n)$ reaches maximum value if m corresponds to delay. However, the accurate time delay between the input and output is not possible to align by finding the exact value of delay due to the resolution. The performance of the pre-distorter model is not significantly affected, when the delay is underestimated up to one sampling period [14, 21].

In order to estimate the pre-distorter with good accuracy, the output has to be normalized by the small signal gain in order to align the power between the pre-distorter and the amplifier. However, pre-distorter often changes the power amplifier input power in order to achieve a certain back-off level at the output. For fair comparison of the DPD performance against the case without DPD, the objective is to keep the output power at the same level with and without DPD. The power alignment between the pre-distorter and the PA can be possible with small signal gain if the PA weakly nonlinearity. However, when the PA is highly nonlinear, the gain normalization depends on the average input power and also the shape of PA nonlinearity [30].

3. WIRELESS TRANCEIVER ON USRP PLATFORM

Software defined radios (SDRs) offer an easily reconfigurable platform for initial prototyping of different things in the wireless communication academia and industry. Earlier, traditional hardware radios were impossible to update according to demand after manufacturing. SDR is a flexible and adaptive communication link for our future communication. Therefore, the communication system can be easily modified to meet the requirements to make a prototyping for different applications. SDR is a concept of getting the code as close to the antenna as possible which turns the radio hardware by simply changing the code [31,32]. For demonstration purposes, SDR platforms offer different levels of prototyping all the way from RF to the FPGA design on the board. In this chapter, we explain USRP transceiver design for DPD demonstration in the SDR platform using Ettus's USRP.

Block chart of a general SDR platform is shown in Figure 16. The structure of the platform is divided into three parts. The right side block represents the RF front end of the hardware which serves as an interface to the analog RF domain. In the middle block, the hardware part is implemented to form the interface between the digital samples and the analog samples. However, the samples by the field programmable gate array (FPGA) are transferred to the host via Ethernet. The left side block shows the baseband signal processing system which is fully designed by the software. Note that, we used MATLAB as a control interface. We can also use another platform such as GNU Radio.

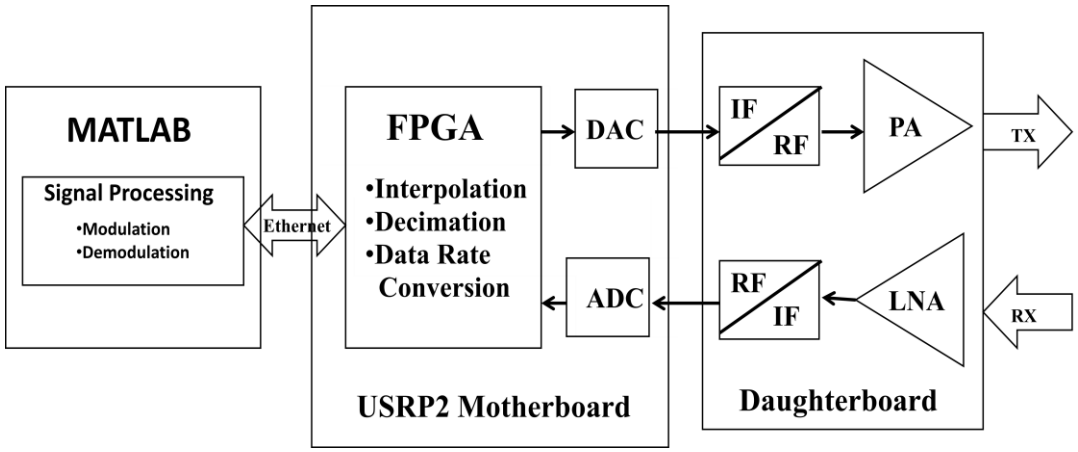

Figure 16. SDR communication system.

3.1. Universal Software Radio Peripheral

The USRP is an open source SDR design platform developed by Ettus Research LLC. It basically contains an RF frontend which has complex electric circuitry for upconverting the IF signal to a RF signal, a digital-to-analog converter (DAC) is responsible for converting digital samples to analog signal, a PA is used to amplify the analog signal for the over air transmission via an antenna. In the USRP receiver, the signal is first amplified by low noise amplifier (LNA) and downconverted from RF to IF or analog baseband. Analog-to-digital converter (ADC) converts the signal to digital domain samples. And FPGA processes the digital samples with the speed of the master's clock rate.

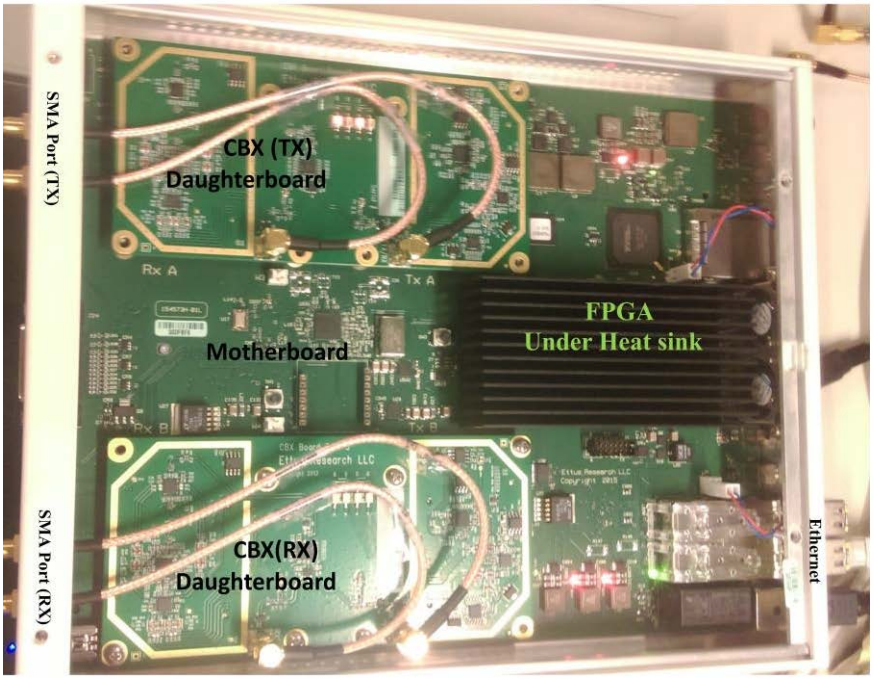

Figure 17. X300 USRP with two CBX-120 daughterboard.

The X300 USRP with CBX-120 daughterboard is shown in Figure 17. Here, the host computer uses SIMULINK and MATLAB to process the baseband signals which are passed to the daughterboard of the USRP through SDRu communication interface. The transmitter and receiver chain of the daughterboard are operated autonomously. In the transmit chain, DAC converts the baseband samples to an analog signal. The analog signal from DAC is directly passed to the receiver chain via wired SMA connector which is connected between the transmit SMA port known as TX/RX and receiver SMA port known as RX2 of the CBX-120 daughterboard. In the receiver side, processing is done in reverse order. The sampling rate was used to calculate by the constant ADC rate divided by the decimation rate which is selected by the users [33, 43].

In this thesis, two different RF daughterboard, i.e. CBX-120 and WBX-120 were used in the same radio, i.e. USRP X300. The X300 USRP with CBX daughterboard were suffering hardware problem in the RX chain. There was a strong LO leakage coming from that RX chain which had a random impact for our results and caused several problems for the data processing. Therefore, the test bench reconfigured by using WBX boards this time instead of CBX. In section 3.2.4 and 3.3.1, we evaluate the transmit and receive chain which is configured by using CBX daughterboard. Due to strong LO leakage CBX daughterboard, we reconfigured X300 USRP by using WBX daughterboards instead of CBX from section 3.4. In order to avoid synchronization issues, we use the daughterboards in FDD mode on the same radio where the interface can stream in the TX/RX and RX2 directions at the specified rates simultaneously. However, some interfaces such as USB 3.0 does not provide separate data paths for transmit and receive chain. In the test bench, we use a gigabit Ethernet connection which is capable of operating in the full duplex mode with a sample rate 200 MS/s for the X300 USRP [34].

The X300 USRP motherboard is used to generate a reference clock to the daughterboard in order to generate LO signals. This oscillator is used to modulate the TX samples from the baseband into the operating TX frequency and the signal from the operating RF frequency to the baseband frequency. The daughterboard can filter the received signal to avoid the aliasing effect from ADC. However, there are few daughterboards known as basicTX and basicRX that provide a direct RF connection to the motherboard and there are no filtering or frequency conversion options [35]. The requested output frequency and sample are obtained by processing the digital sample values with digital down converters (DDC) where digital samples from the ADC are decimated to the desired baseband frequency to create I-Q data. This decimation is performed when the sampling rate f_s divided by the decimation factor. The digital upconverter (DUC) also works in the same way but in reverse order where the sampling rate f_s multiply by the interpolation factor [36].

3.2. USRP Daughterboard Performance

The selection of most appropriate RF daughterboards in order to use in the USRP is mainly based on the application requirements, frequency range, bandwidth and number of channels. The possibility to utilize the full bandwidth in the USRP often depends on the daughterboards and also the resolution of the data transferred through the host interface. The daughterboards using reference clock for the USRP which can be used for the multiple input and multiple output (MIMO) application by performing the simple clock alignments. However, phase alignment between the RF chains is not available in all daughterboards. The BasicRx, BasicTx, LFRX and LFTX daughterboards do not include the LO that contribute to phase ambiguity between the RF channels. The SBX daughterboards use phased locked loop (PLL) which have resynchronization option to align the LOs by the timed serial peripheral interface (SPI) commands. On the other hand, all other daughterboards required channel to channel phase calibrations after each PLL retune [47]. The table 1 shows the USRP daughterboard properties for different USRP daughterboards.

Table 1: USRP daughterboard properties [47].

Daughterboard	Frequency Range	Bandwidth	Area of Application
WBX-120	50 MHz - 2.2 GHz	120 MHz	GPS,GSM, VHF, TV Broadcast, Amateur Radio
SBX-120	400 MHz -4.4 GHz	120 MHz	GPS, GSM, WiMAX, Radar
CBX-120	1.2 GHz - 6 GHz	120 MHz	GPS, WiMAX
UBX-160	10 MHz - 6 GHz	160 MHz	GPS, GSM, WiMAX, VHF, Radar, Amateur Radio

3.3. USRP Transmitter

The 16 QAM signal is transmitted from the USRP transmitter to receiver through a wired channel. The transmitter divided into two-part, one is SIMULINK model of the transmitter with SDRu transmitter interface and other is the USRP hardware. In the baseband transmitter SIMULINK model, a random binary data sequence is continuously generated data frames. After that, the 16 QAM modulator block conveys source information by changing the phase of the carrier signal. Next, the pulse shaper is used to generate the data bits. Then, the signal is oversampled and pulse shaped in order to reduce the spectral regrowth of the digital processing. Finally, the SDRu transmitter block establishes a link between baseband transmitter SIMULINK to USRP hardware. Figure 18 shows a SIMULINK test bench. The test bench is a combination of SIMULINK based signal processing and the USRP interface. At a certain operating point, the signal power of the waveform after root raised cosine transmit (RRC) filter is -8.59 dBm. After passing the gain blocks the signal power level is -23.59 dBm which reduce the power level around -15 dB. It means that we can control input power level in the transmit chain by using the gain block in the MATLAB. Note that, we set 30 dB to transmit gain in the SDRu communication block (usually in the daughterboards of USRP) to obtain a better signal.

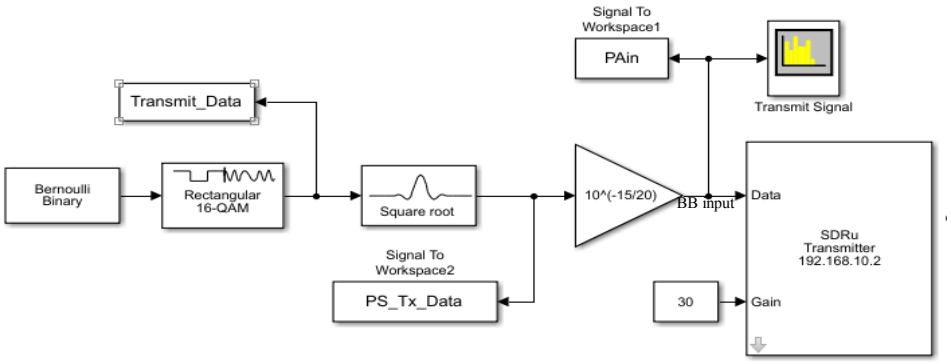

Figure 18. 16 QAM transmitter SIMULINK test bench.

3.3.1. Digital Modulation

A random binary data sequence is generated with a sample time $2\,us$ to set the generator to produce bits at a sample rate of 500 kbps. The samples per symbol are four that make output 4 bit per symbols to pass 16 QAM modulator. In order to set up a communication system with varying envelope waveform, a 16 QAM modulation scheme is chosen. 16 QAM is a digital modulation scheme where the sample conveys the source information by changing the phase of the carrier signal. The information is conveyed by mapping binary data bits to symbols where the modulation scheme defines the method of the mapping bits to symbols. A high interpolation or decimation rate can generate fewer samples. The sampling rate and RF bandwidth related by interpolation or decimation factor. The sampling rate was used to calculate by the constant ADC rate divided by the decimation rate which is selected by the users. Here, the sample time is the inverse of the sample rate of the system which must be followed by the Nyquist theorem.

3.3.2. RRC Pulse Shaping Filter

The root raised cosine transmit (RRC) filter interpolates the data frames in the SIMULINK transmitter model. The RRC filter is also known as a pulse shaper that is used to transmit digital signal with constrained bandwidth to reduce the intersymbol interference (ISI). The role of the pulse shaping filter is to limit the bandwidth of the signal such that it meets the applicable spectral mask by filtering out spectral components. However, the roll-off factor (β) is also indirectly responsible for specifying the bandwidth (β/2T) of the filter, where T is the symbol period. Hence, pulse shaping slightly increases the channel bandwidth of the signal to reduce power at the adjacent channel bands. Here, each sample entering to the RRC filter becomes 16 samples at the output. For example, 4 samples per frame fed to RRC filter 4×4=16 samples at the output. We calculate the time required to transmit a single frame of data which is the product of frame size and sample time. Figure 19 (a) and 19 (b) shows the frequency and time domain representation of a pulse shaping filter, respectively. We notice that if we increase the roll-off factor, the power at the adjacent channels decreases. On the other hand, reducing the roll-off factor increases the signal bandwidth.

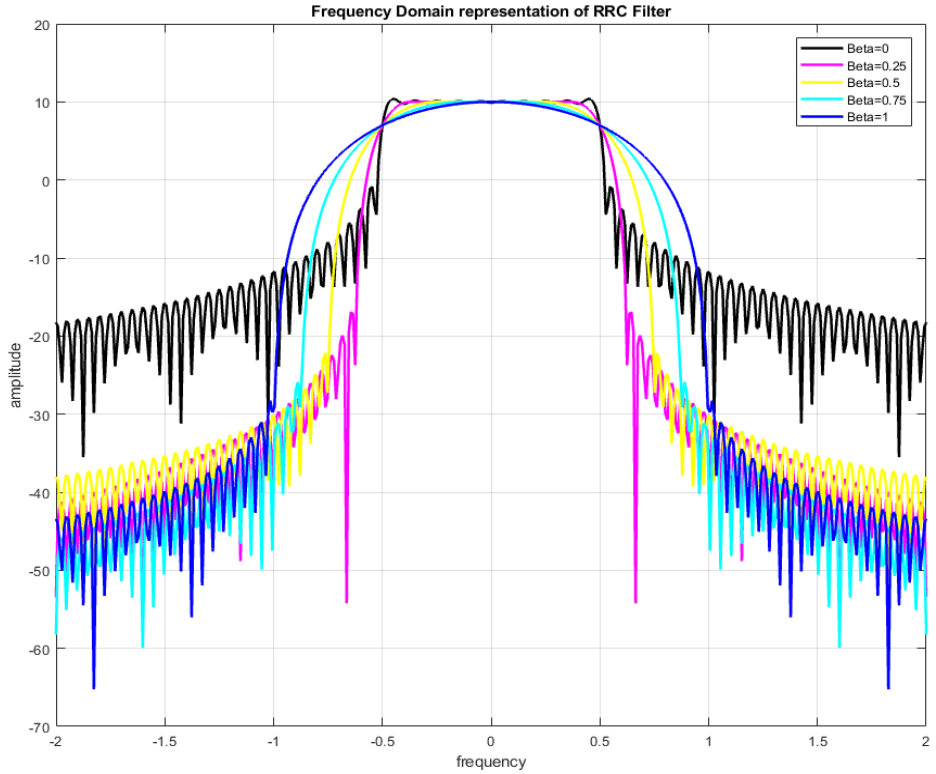

(a) Frequency domain

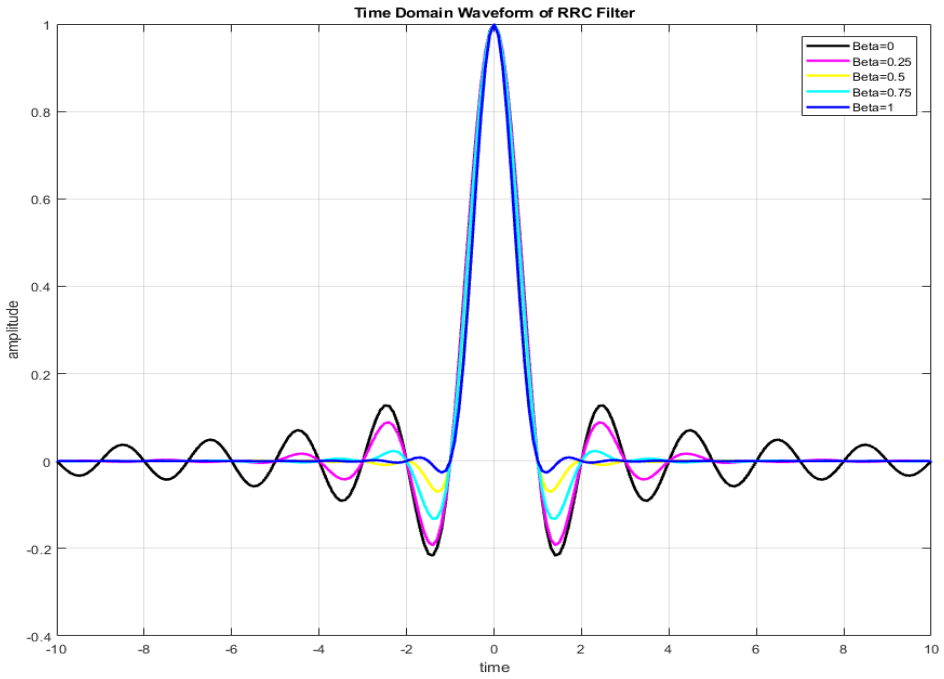

(b) Time domain

Figure 19. Pulse shaping filter.

3.3.3. Interface of Commercial USRP

The Ettus provides the necessary support to interface with a USRP hardware driver (UHD) of the USRP. This is a C++ interfacing library which makes the switching between real and complex samples, set the operating frequencies, amplification sends and receives the samples from the buffer of the device. The UHD contains own internal buffer of the Ethernet connections which operates the data streams. There are different ways to access the USRP. SIMULINK provides a graphical user interface (GUI) for controlling the USRP platform. The USRP transmitter can be accessed through SDRu transmitter bock that can set up a link between the baseband SIMULINK transmitter model and USRP hardware digital and RF front end via Ethernet subnetwork.

Initially, we install a communication system toolbox in the MATLAB to establish connectivity. After download and install the supported package, we can verify the connectivity by typing 'findsdru' in the MATLAB command window. In order to establish a successful connection, the IP address of the USRP is required to be recognized by the host computer and one should be able to ping it from the computer. The USRP should be configured to the centre frequency of the transmission which should be in the range 1.2 GHz to 6 GHz for CBX-120 daughterboard. Note that, 'LO Offset' should be fixed properly to remove of harmonics generated by the USRP that would interface the actual signal. The UHD software used self-calibration to minimize the LO offset. In the typical use-case, the user specifies the centre frequency for the signal chain. The RF front end will tune as close to the centre frequency. On the other hand, the DSP will account tuning error between the target frequency and the actual frequency. We can also move the DC component out of our band-of-interest by using UHD software advance tuning. The advance tuning can be done by passing the desired LO offset to the 'uhd::tune_request_t' object. The object uses integer-N tuning instead of the default fractional tuning in the specific daughterboard for better spur performance [63, 64].

In the test bench, we use SMA cable between the transmitter and receiver SMA ports. As high transmit power might damage the receiver, we placed 40 dB attenuator to keep the received signal under the damage level. The maximum achievable transmit power is from 12 dBm to 22 dBm over the frequency range of 1.2 GHz to 6 GHz while the maximum input power to the CBX is -15 dBm. The receiver gain control parameters and linearity are explained and discussed later in the following chapters. The specification of WBX and CBX daughterboards shown in table 2.

Table 2: WBX and CBX daughterboard specification for X300 USRP [37, 38].

Parameter	**CBX**	**WBX**
Frequency	1.2 GHz ~ 6 GHz	50 MHz ~ 2.2 GHz
Master Clock Rate	200 MHz	200 MHz
Maximum Input Power	-15 dBm	-15 dBm
Transmitter Gain	31.5 dB	0 ~ 25 dB
Receiver Gain	31.5 dB	0 ~ 31.5 dB
Maximum Tx Power	12 ~ 22 dBm	12 ~ 18 dBm
Bandwidth	40 ~ 120 MHz	40 ~ 120 MHz

3.3.4. Evaluation of Transmit Chain

A SIMULINK based test bench combined with a signal analyzer (Rohde & Schwarz SMIQ06B) was used to evaluate the nonlinearity of the transmit chain of the USRP. The test bench for the measurement is shown in Figure 20. Here, SIMULINK model in host computer operates as a baseband, X300 USRP with CBX daughterboard as RF front end. The spectrum analyzer which is feedback the measurement data to the host computer using standard commands for programmable instruments (SCPI) commands form the MATLAB scripts through the general purpose interface bus (GPIB) device. The motherboard of the X300 USRP is configured with two CBX daughterboards for this test bench. The CBX daughterboards allow full duplex operation modes if the transmit port connected to TX/RX port and receiver port is set to RX2. However, this test bench only configures for the transmit chain. In order to analyze the measurement data, the GPIB interface is established between the host computer to a spectrum analyzer. Here, 10 MHz reference clock is connected between the spectrum analyzer and the USRP in order to avoid frequency error [49].

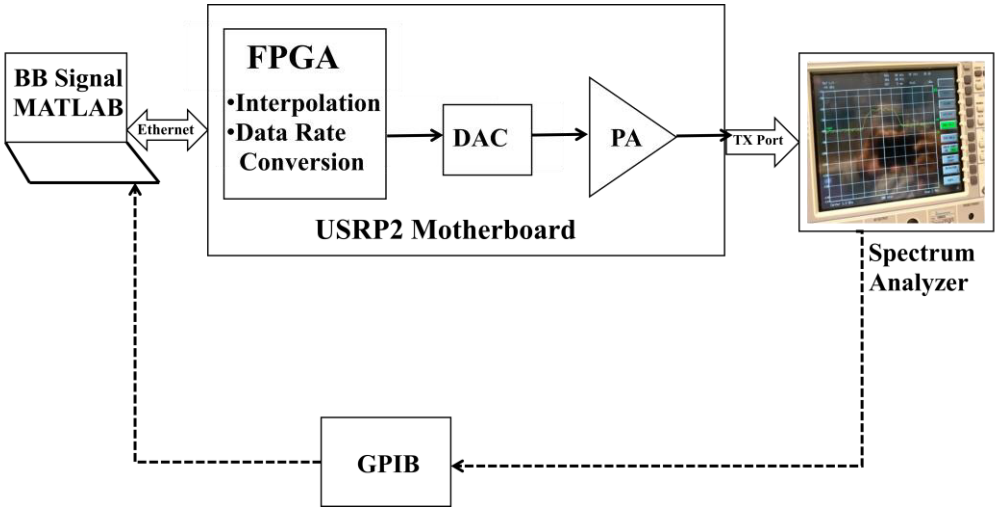

Figure 20. Block diagram of transmit chain.

In the test bench, the gain of GVA-84+ monolithic internal PA of the CBX daughterboard is around 22 dB at 1.3 GHz centre frequency. The output power of the 1 dB compression point, saturation point and also third order interception point of the GVA-84+ monolithic internal PA are around 20 dBm, 22.3 dBm and 36 dBm respectively at the same centre frequency [39].

The spectrums measured at the PA output with different input power levels are plotted to figure 21. As expected, more power is spread to the adjacent channels as the input power of the PA is increased. The reference signals power in a particular operating point form the MATLAB is -23.59 dBm and the transmit gain on the CBX daughterboard is 30 dB. Therefore, the signal power level we can assume around -23.59 + 30 = 6.41 dBm. There might be 3 dB cable losses in the test bench. The input power level in the PA is around 3.4 dBm. By using the spectrum analyser which actually feedback the measurement data to the host computer, we calculate the output power of the PA is 16.13 dBm. In this circumstance, PA has the gain around 13-16 dB depending on loss in the system.

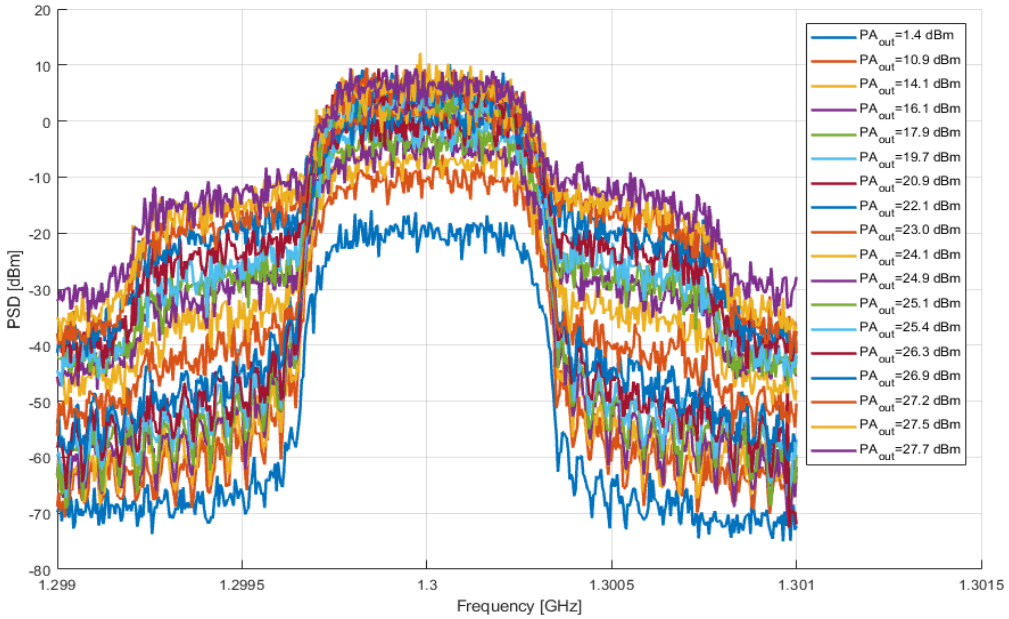

Figure 21. PSD of transmit chain.

Figure 22 illustrates the power sweep of the USRP transmitter. Here, the RMS input power sweep in order to measure the RMS output power of the modulated signal. As power is increased, the gain is reduced. The gain in the transmitter is around 10 dB. The 1dB output compression point is approximately 25 dBm. In order to overcome the nonlinearities of the PA, digital pre-distortion is applied later on in the thesis.

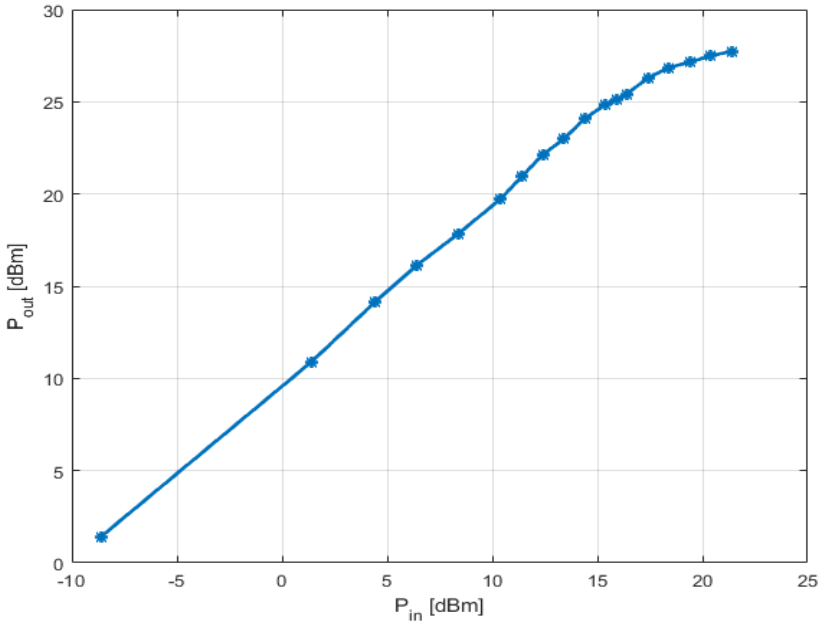

Figure 22. Power sweep of the USRP transmitter.

Figure 23 presents the main channel, upper adjacent channel and lower adjacent channel powers as a function of the PA input power, respectively. The adjacent channel power integrated over -587.5 KHz to +587.5 KHz frequency range. Different operation regions can be detected from the figure, i.e. 1x and 3x. In the 1x region where the adjacent channel power has appropriately the same slope as the main channel, the noise is dominating in adjacent channels and hence the nonlinearity is not seen or cannot be measured. When increasing the power more, first adjacent channel power starts to rise above the noise floor. In this 3x region, the slope of the ACP is approximately 3x the slope of the channel power. Due to the third order nonlinearity the 3x slope is different.

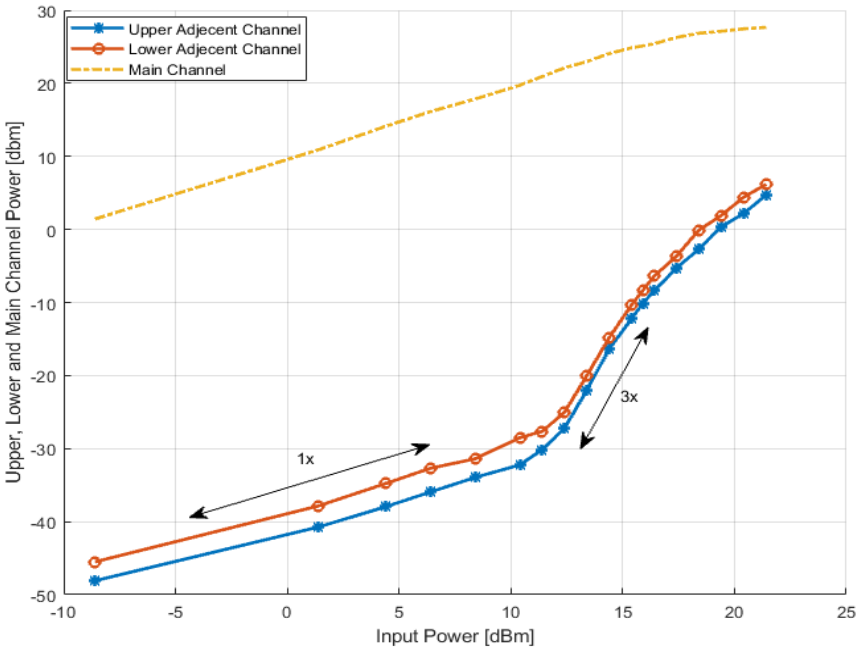

Figure 23. Upper, lower and main channel power for different input power.

3.4. USRP Receiver

The purpose of the SIMULINK receiver model is to receive the transmitted signal with the USRP hardware interface. It consists of two subsystems one is SDRu receiver interface subsystem and another one is the enabling hold subsystems. The SDRu receiver interface subsystem is responsible for tunning the centre frequency, receiver gain and also for the downconversion. The downconversion should be matched with the SDRu transmitter hardware interface block in order to transmit and receive the data with same I-Q sample rate. In the figure 24, SDRu receiver block established a link between the receiver SIMULINK design and USRP hardware via Ethernet. This block also controls the transmit data from the radio using the USRP hardware driver (UHD). In the SDRu receiver block, there are two output ports. One is referred to as data which is responsible for receiving data from the radio while the other one is the data length port that provides a column vector signal with a fixed length. Finally, the enabling hold subsystem processes the received data.

The enabling hold subsystem is required in order to sample the received waveform at the correct time instant. Figure 25 shows the timing diagram of digital data with the strobe. In the timing diagram, we notice that the input samples are passed through input to output if the strobe is high. Otherwise, it holds the previous value that value until the strobe signal is decreased. The strobe is an enable signal for the time error detection which is derived from decrementing module-1 counter [40]. The data on the adjacent parallel lines is sent by using the strobe signal.

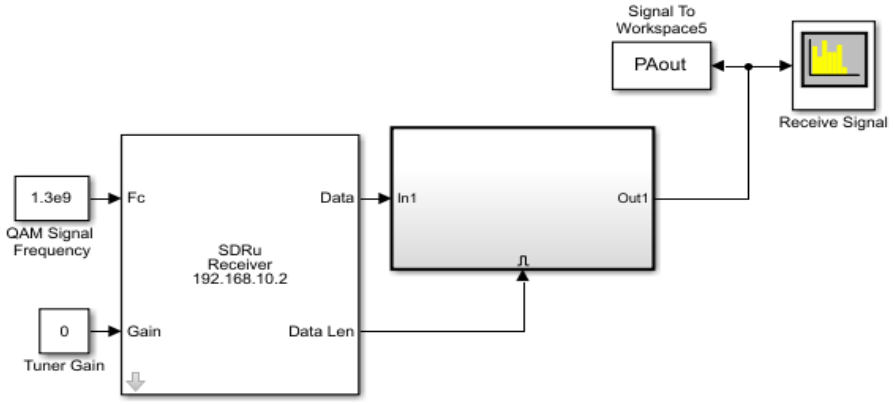

Figure 24. 16-QAM receiver SIMULINK model.

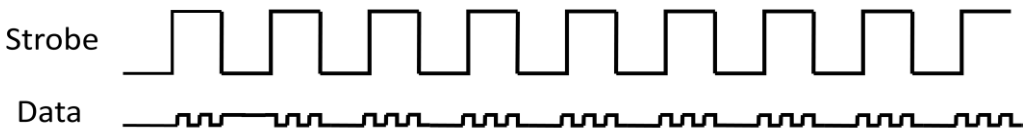

Figure 25. Timing diagram of digital data with strobe.

The USRP transmitter and receiver are suffering from frequency offset and synchronization errors. Therefore, synchronization is required to be done before successful data capture. Also, frequency offset occurs when a difference exists between the transmitter and receiver oscillator frequencies. During the operation system must follow a known phase relationship between the transmitter and receiver in order to align the sample time and clock. The PLL causes the phase ambiguities for the interpolation and decimation. Therefore, calibration is needed to compensate for the phase offset and make proper synchronization. Most of the RF daughterboards uses a fractional-N synthesizer [2,47]. This fractional-N synthesizer introduces a random phase offset in each return which is used to generate the local oscillator (LO) signals. In order to align the phase between the RF channels, the phase offset caused by the passive components is needed to be measured and compensated between the RF frontends. The daughterboard such as CBX and WBX does not have resynchronization feature which resets a fixed offset after each time turn on the USRP power. Hence, the offset in terms of delay and phase varies in each round when configuring with the USRP from SIMULINK.

Third option for USRP X300 daughterboard is called SBX [41] has features which would enable the proper, fixed and stable synchronization. SBX board would be most suitable for linearization demonstration. As SBX boards were not available during the thesis working period, WBX and CBX daughterboards where used instead. SBX has a PLL which integrates a voltage control oscillator (VCO) having resynchronization feature in order to fix the phase. The VCO actually lock the phase of the generated frequency with respect to the reference frequency. This SBX daughterboard is not required to be calibrated after each retune, but it is necessary to calibrate it periodically. So far SBX daughterboard would be an ideal option for example for phased array applications within the limited frequency range. Some other available daughterboards such as BasicRX/TX and LFRX/TX daughterboard has phase errors due to the absence of LO signals [33].

3.4.1. Evaluation of Receiver Chain

In this test bench, Rohde & Schwarz SMIQ06B signal generator is used to generate an arbitrary waveform which has own sampling clock, RRC filter and modulation settings. The centre frequency applied to the signal generator and the USRP receiver is 1.3 GHz, respectively. Attenuation around 40 dB connected between the TX port of the signal generator and the RX port of the USRP. The signal generator generates an arbitrary waveform to the receiver chain of the USRP daughterboard. Finally, the samples are stored to MATLAB workspace. Figure 26 shows the block diagram of the receiver chain.

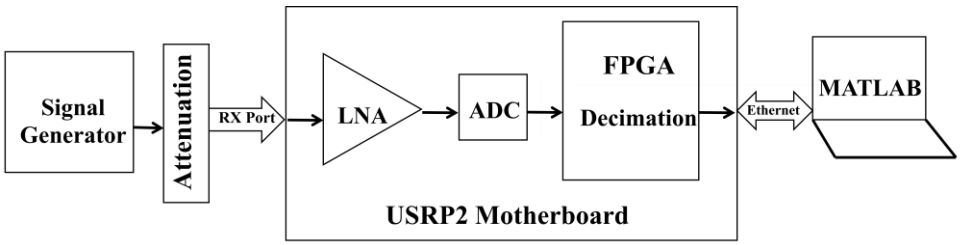

Figure 26. Block diagram of receiver chain.

Before moving on to the linearization demonstrations, it is important to make sure that the receiver chain is linear enough. In other words, the receiver chain should be linear or should not induce any kind of nonlinearity which would have an impact on the linearization performance. On the other hand, the received signal should have enough signal to noise ratio (SNR) in order to characterize the nonlinear behavior. The PSDs measured in different RX power levels are shown in Figure 27. We noticed that there are no significant impact of in-band and out-band distortion on the PSD at different RX power levels with the measured input powers. For efficient DPD demonstration, the receiver gain of the USRP is more than 10 dB (above noise floor) in order to get a better signal in the output. The AM/AM characteristics of the receiver chain in figure 28. During the measurement, we did not measure the data up to the 1 dB compression point which is one of the measurement errors.

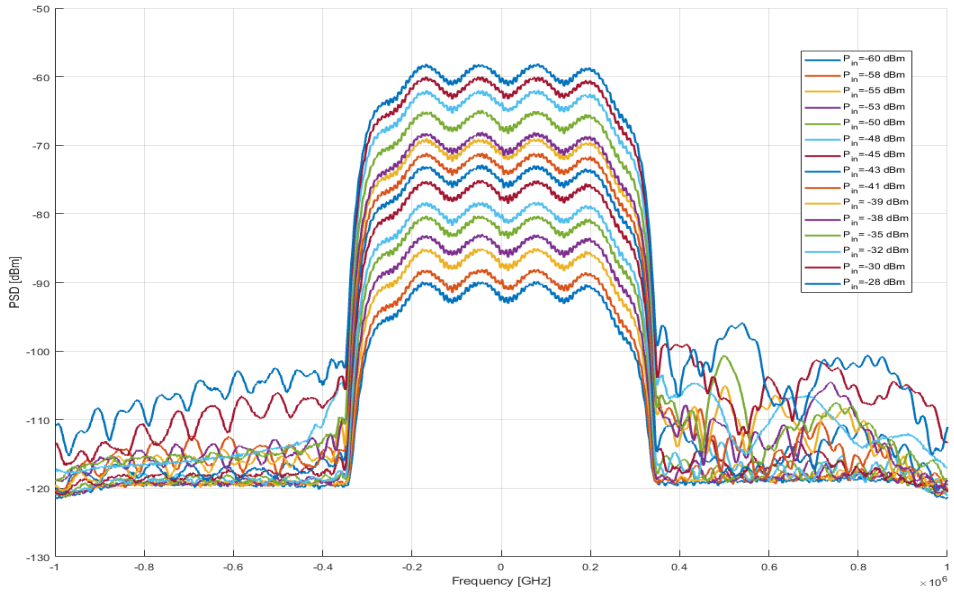

Figure 27. PSD of receiver chain.

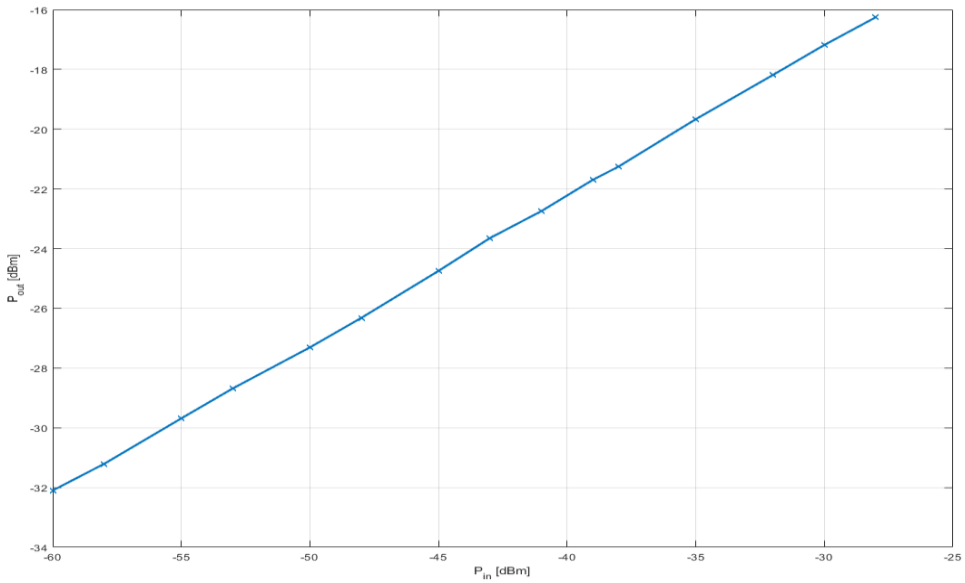

Figure 28. AM/AM of receiver chain.

3.5. System Performance Analysis of Transmitter Test Bench

Several factors may impact the performance analysis of a transmit system when designing an efficient high-speed transmitter. The feasibility of any given system requires a proper top-level system performance. An analysis helps to understand the trade-off between various factors of the system cost and the level of reliability [42]. In this thesis work, the X300 USRP with WBX daughterboard used in this thesis in order to guarantee correct operation point for the measurement receiver and transmitter. Figure 29 shows the PA test bench with a measurement receiver.

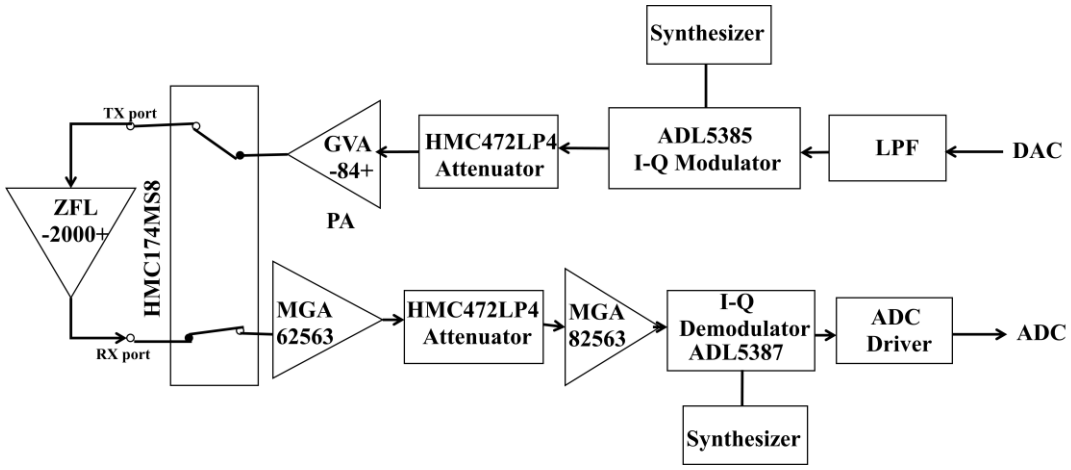

Figure 29. PA test bench with measurement receiver.

The 16 QAM test signal with -24.7 dBm input power is fed to the USRP transmit chain. The transmitter gain for the WBX daughterboard is 30 dB. Therefore, the transmit port power or input power for the external PA is around 2.2 dBm. Here, we approximated 3 dB cable and connectors losses. The maximum output power of the external PA is around 16 dB at the 1.3 GHz centre frequency [20]. The attenuation between the output of the PA and RX port of USRP is 50 dB. Finally, the received signal power approximately -29.8 dBm. The receiver gain was set to zero in order to capture the transmitter power. Table 3 illustrates the link budget for X300 USRP with WBX daughterboard.

Table 3: Link budget calculation.

Element	Value
Test signal power at input (DAC output)	-24.7 dBm
Transmitter gain (WBX Daughterboard)	+30 dB
PA input signal power	+ 5.3 dBm
External PA gain (at 1.3 GHz)	15 dB
Attenuation	+50 dB
Cable and connectors loss	3 dB
Receive signal power	-29.8 dBm

4. DIGITAL PRE-DISTORTION USRP PLATFORM

The demonstration of the DPD is performed in the SDR platform, i.e. USRP X300 where WBX daughterboard is used as a RF front end. Chapter 3 already mentions that the WBX daughterboard contains two different antenna ports. The TX/RX port can be used in full duplex mode while RX2 port works only in the receiver model. With two WBX boards used in two channels of the USRP X300 motherboard, we can use one WBX daughterboard as the transmitter while the other one is used as measurement receiver. Hence, the same USRP platform can work on both modes simultaneously and hence the DPD can be demonstrated in a single USRP device. By demonstrating the DPD by just one physical USRP device, we can simplify the synchronization and potentially achieve more accurate results. However, WBX cards are still suffering from non-fixed phase reference which means that we needed to align the symbols, i.e. synchronization in after each set of samples transmitted from SIMULINK to the USRP based link back to SIMULINK. The software part of the demonstration is developed on SIMULINK by using SDRu communication blocks to interface between USRP and the software. This chapter presents the measurement setup of the DPD scheme in order to create the nonlinear model of the PA and measure the performance of the DPD. In the first phase, an overview of the test bench is presented. Later on in the chapter, the DPD performance is analyzed based on the experimental results.

4.1. Test Bench

A block chart of the DPD demonstration platform is illustrated in figure 30. The DPD demonstration platform consists of a host computer and USRP X300 connected via an Ethernet cable. Spectrum analyzer is used only to observe the signal spectrum during the operation, but not to sample any signal for the feedback used for DPD. The USRPs WBX daughterboards are configured to work as RX and TX. An external PA (ZFL-2000+) is used in TX. The specifications of the PA [20] are given in Table 5. The PA output is divided to a spectrum analyzer and to an external attenuator which is routed to the measurement receiver operating in the same USRP as the TX. The spectrum analyzer is used to verify the measurement results and observe the results in real time. The models of the used measurement equipment are given in Table 4.

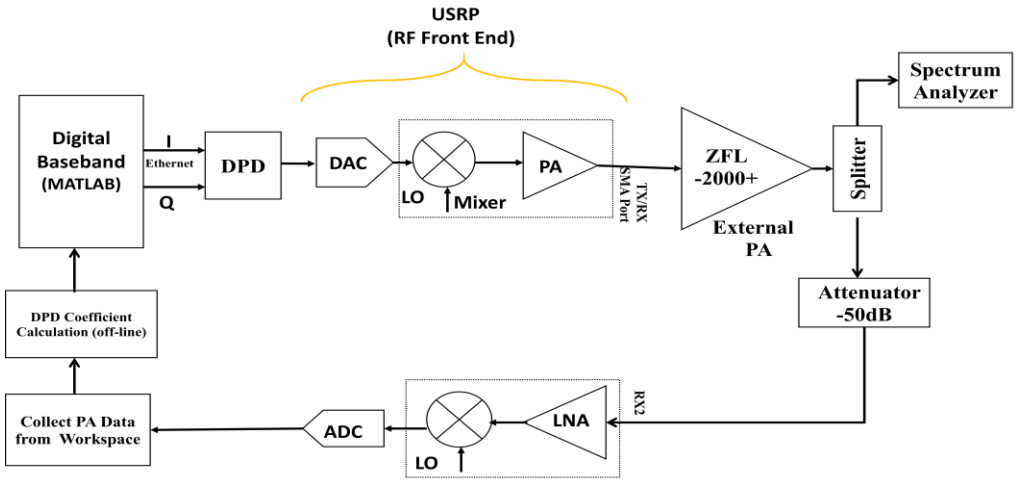

Figure 30. Digital pre-distortion scheme.

Table 4: Measurement instruments.

Instruments	**Model**
Signal Generator	Rohde & Schwarz SMIQ06B
Signal Analyzer	Rohde & Schwarz FSIQ7
SDR	Ettus X300
DSP	Ettus WBX
GPIB	NI (GPIB-USB-HS)
GPIB Connector	IEEE-488
Interfacing	MATLAB R2017b

Table 5: Power amplifier electrical specification [20].

Model No	ZFL-2000+
Frequency (MHz)	10 MHz to 2000 MHz
Gain (dB)	20 dB
Maximum Output Power (dBm)	+16 dBm
Maximum Input Power (dBm)	+5 dBm
DC Voltage	15 V
DC Current	120 mA

4.2. Measurement Results

In this section, we present the measurement results of the DPD performance on the USRP platform. The 16 QAM input waveform generated from the SIMULINK which is pulse shaped by the RRC pulse shaping filter (roll-off factor of 0.35). The symbol rate of the input waveform is 500 kHz and 4-times oversampling is used in pulse shaping as well as in the measurement receiver. In the transmitter and receiver chain of the USRP daughterboard, we applied 1.3 MHz carrier frequency and also 4 MHz local offset. The static DPD model used to extract the coefficient for the pre-distorter parameters for the DPD. Figure 31 shows the SIMULINK model of the transceiver with the DPD for the measurement.

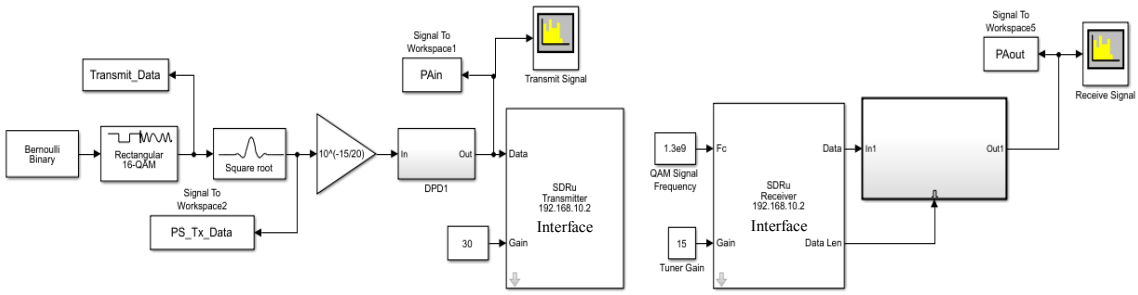

Figure 31: SIMULINK model of transceiver with DPD for measurement.

4.2.1. Deriving DPD Coefficient

To linearize the output of the PA, we consider static DPD design which was explained in chapter 2. In the static DPD model, we consider the memory depth ($M = 3$) and degree of a polynomial ($K = 3$) which produces $K \times M = 9$ complex coefficients to provide decent linearization performance. The training length is 2000 to calculate the DPD coefficient offline. Figure 32 shows the amplitude of DPD coefficients with respect to memory depth and polynomial order. If we increase memory depth then the linearization will be better. In our test setup, the used bandwidth was relatively narrow and hence significant memory effects were not present.

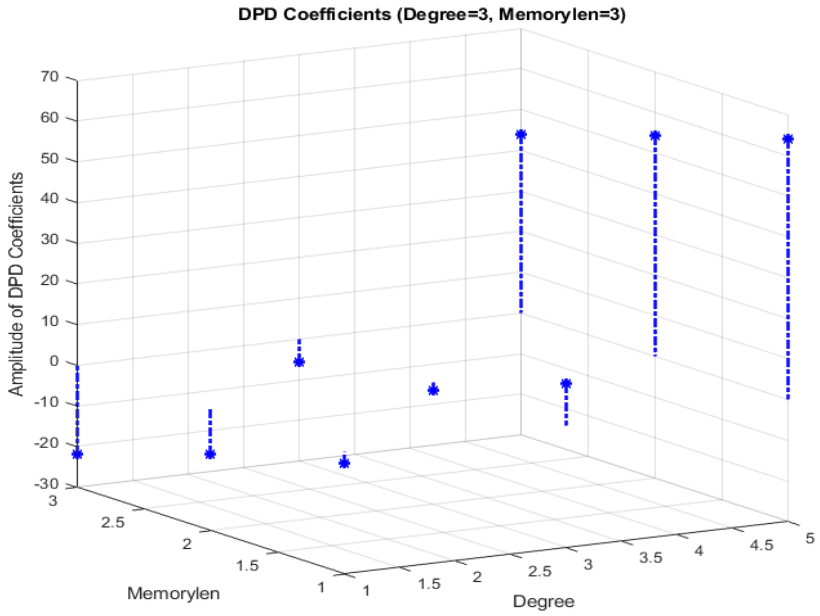

Figure 32. Amplitude of DPD coefficients.

Figure 33 shows the amplitude of the impulse response extracted for each order of nonlinearity. Impulse response with several nonzero taps indicates memory of the system. In the figure, the profile of the coefficients over the memory window for different orders of the nonlinearity is similar. This indicates that most of the memory content does not depend on the nonlinearity. Hence, such the system could be modelled e.g. by Hammerstein type of model (Chapter 2) where the nonlinearity is static and followed by a linear filter which models the memory.

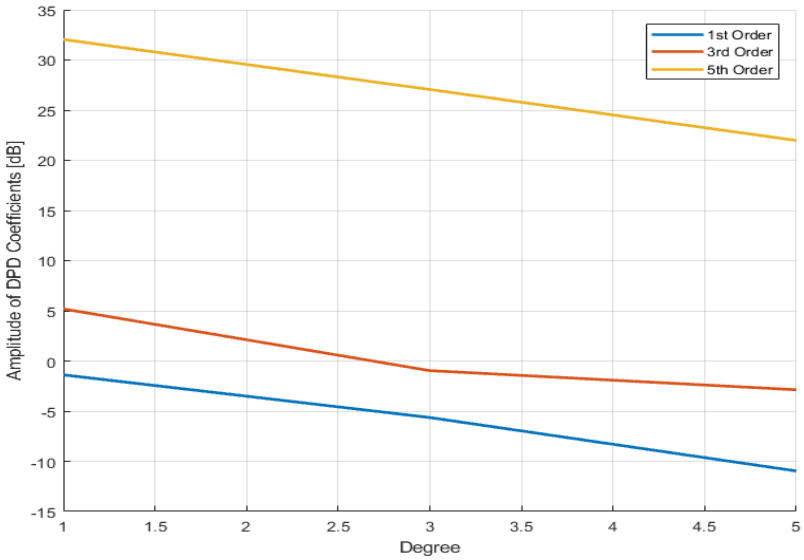

Figure 33. Order of nonlinearity of DPD coefficients.

4.2.2. Example of AM/AM and AM/PM Characteristics of the PA and DPD

In the DPD linearization technique, the inverse nonlinearity of the PA is cascaded with the PA in the transmit chain such that the output of the PA gives a linear output. In other words, the input signal is fed to the pre-distorter before the PA. Figure 34 presents the AM/AM characteristic of the PA output with and without pre-distortion. The maximum values of all the curves in the figure are normalized to one to illustrate the behaviour. The blue curve shows that the PA is suffering from compression without DPD. The green curve is the output of the DPD which is observed to have an expansive shape. The shape is having an inverse form compared with the raw PA response without DPD. The red curve shows the output of the linearized PA. Finally, DPD achieved the required linear output response from the PA as we expected, i.e. blue curve. Hence, the pre-distorted signal of the PA is cascaded with the output response of PA to make a linear output response.

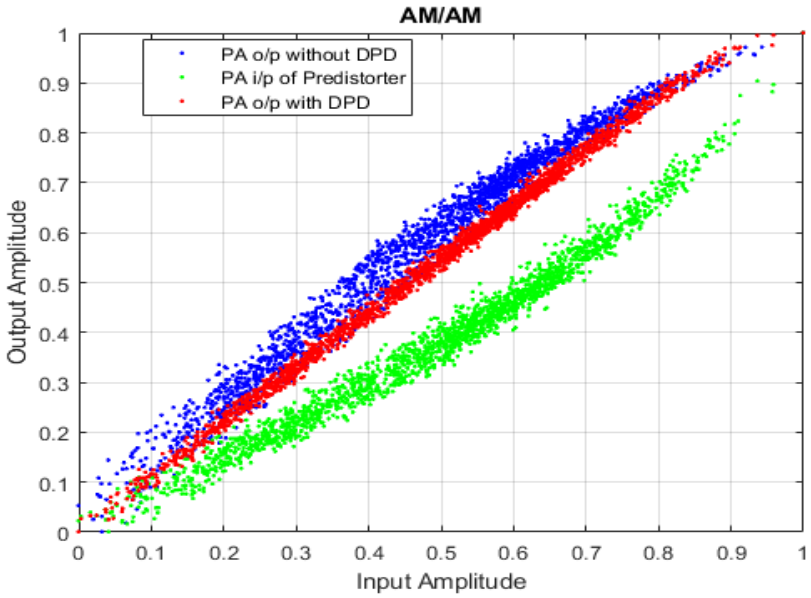

Figure 34. AM/AM response of PA with and without DPD.

Figure 35 shows the AM/PM characteristic of the PA output with and without pre-distortion. The input power fed to the external PA is around +2.2 dBm. Without linearization, the AM/PM is spread especially with lower input values. The spreading of the low amplitude values in phase does not have a significant impact on the system level performance due to the fact that those values do not contain significant information of an oversampled signal. However, the spreading of the phase can be considered to be an indicator of some memory present in the system. The DPD is able to narrow the spreading of the phase over the input amplitude. Hence, also AM/PM is linearized by the DPD. Very low amplitude values of the input signal do not have a significant impact on the signal quality as they are anyway below the noise level of the signal.

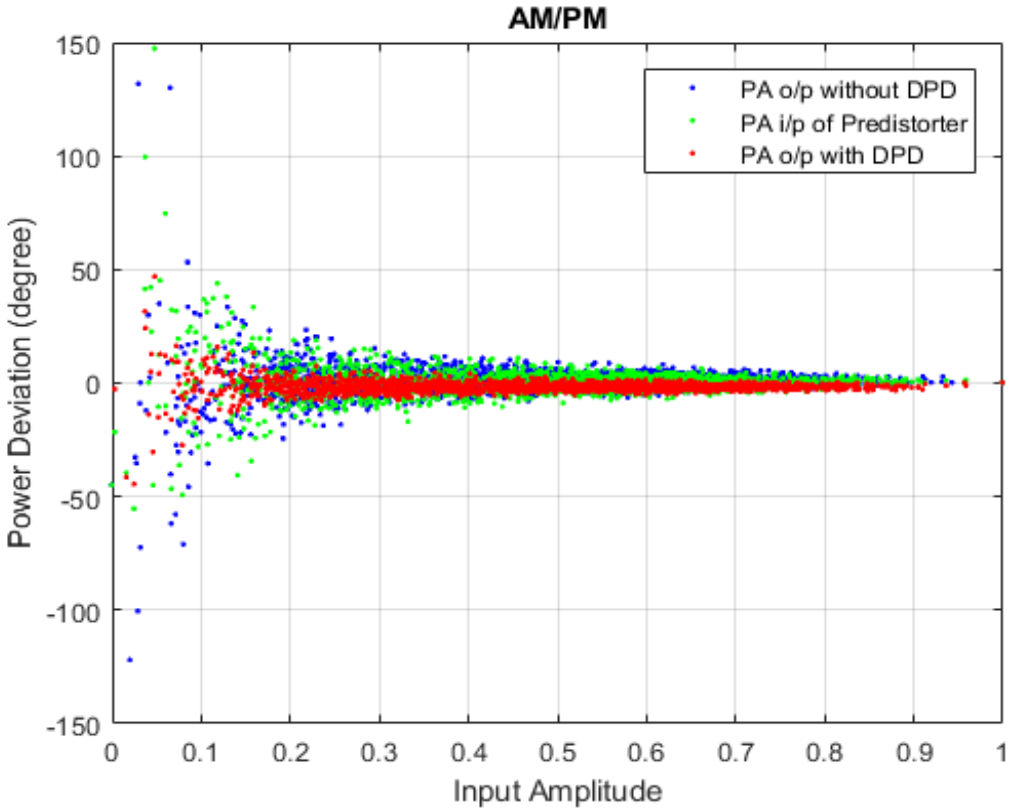

Figure 35. AM/PM response of PA with and without DPD.

4.2.3. Example of Measured Spectral Regrowth

The PSD measured at the input and output of the PA is shown in the figure 36. Also the spectrum with DPD is plotted to obtain the observed ACPR improvement. The spectrum is plotted in MATLAB based on the measured values by USRP. Hence, the level of PA output PSD is lower than the PA input PSD due to attenuator used in the feedback branch. We also observe that the output of the PA is suffering from spectral regrowth. Here, the ACPR is increased due to the nonlinearity. However, the spectral regrowth is suppressed due to the pre-distorted input in the PA. Finally, the demonstrated static DPD scheme is reducing ACPR about 10 dB in the chosen operation point. ACPR illustrates the ratio of the main channel concerning the ACP. The channel offset between the main channel and the adjacent channel is 87.5 kHz. The channel offset is half of the roll-off and bandwidth multiplication. As we seen in the figure, the green PSD curve shows the reference signal is fed to the PA. The red PSD curve shows spectral regrowth due to out-of-band distortion. Finally, the blue PSD curve is the output of the DPD which reduce the ACP.

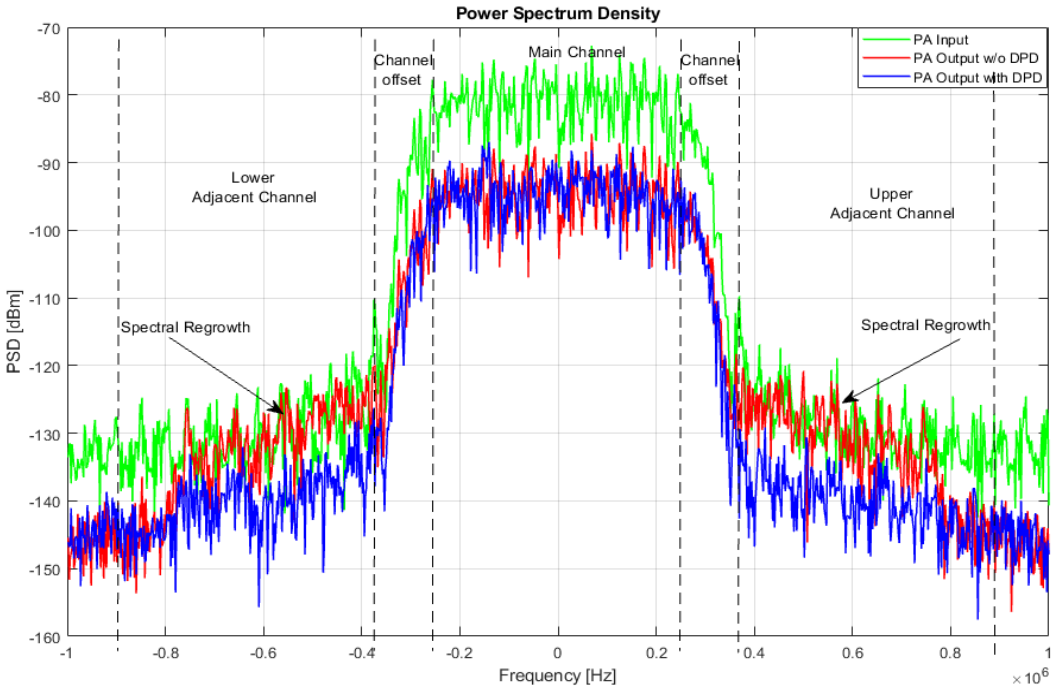

Figure 36. Power spectrum density.

4.2.4. Example of EVM

Figure 37 presents the EVM for the received symbols with and without DPD respectively. As we have seen in the figure, the constellation points are slightly compressed in the edges. The frequency responses of the device are presented mostly. In this example, the difference between the received and transmitted symbols divides by the average value of the input signal presents EVM. Before normalizing the receiver signal, received symbols has to be derotated so that they are aligned in the constellation [12]. The reference input 16 QAM signal from the MATLAB with -24.7 dBm input power feds to the USRP which achieves an EVM approximately 2.1% with DPD. However, at the same power level, EVM is 7.6% without DPD. The input power of the PA is around 2.2 dBm. The external PA has the gain of approximately 15 dB. Hence, EVM improvement achieved using memory dependent DPD, where memory dependency is able to also replace the traditional equalization in this case. Note that, at this operating power the transmitter gain for the USRP is 30 dB, and the receiver gain for the USRP is kept as zero.

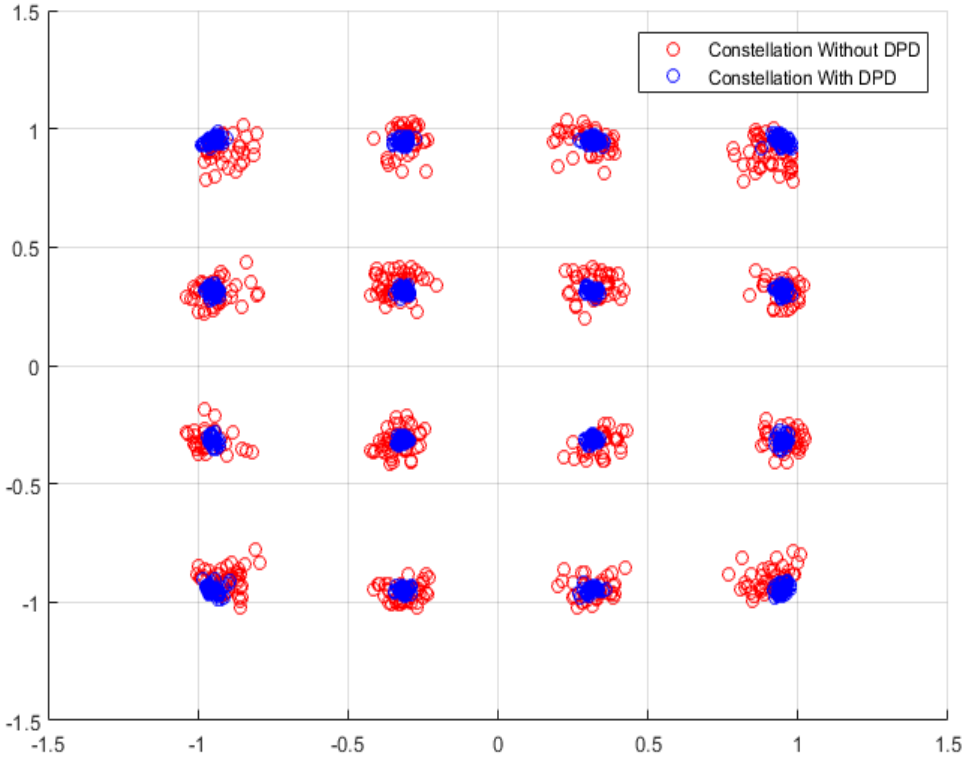

Figure 37. 16 QAM signal with $P_{out} \approx$ 17.2 dBm power for EVM.

4.2.5. Power Dependent DPD Performance

In this thesis work, the performance of the DPD is analyzed by driving the PA in different power levels. The measured ACPR with respect to different output is shown in figure 38. It can be observed that without DPD the ACPR is increased proportionally to the output power. However, after applying the DPD, ACPR reduce that means out-band distortion due to the interference of the adjacent channel is decreased.

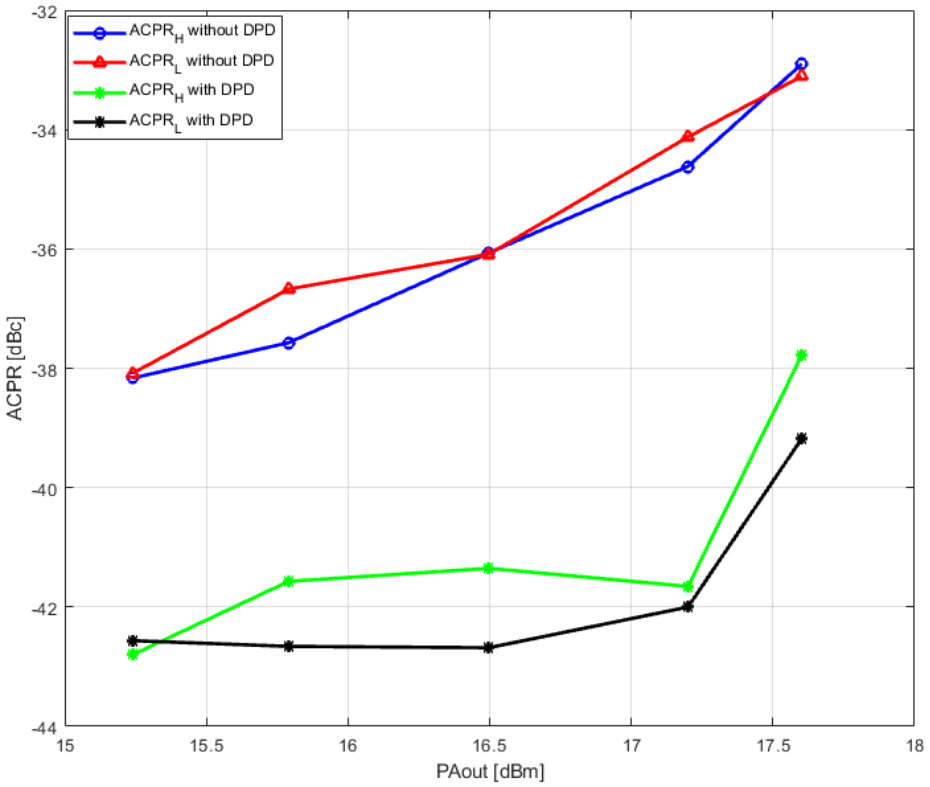

Figure 38. ACPR with respect to PA output power with and without DPD.

EVM as a function of PA output power with and without DPD is shown in figure 39. As we seen in the figure the DPD reduces the in-band distortion. It seems that the window where DPD is working correctly is very limited due to different RX gain RX daughterboard. This is because of the error in the Rx gain control. During the measurement, receiver gain for the RX daughterboard is zero. Therefore, the DPD is working very limited region. We can solve this problem by increasing the receiver gain of the RX daughterboard. In other words, Rx should have been configured to have more gain such that the signal to noise ratio of the received signal would be enough for DPD coefficient calculation. Hence, a proper automatic gain control (AGC) should be implemented to the receiver to achieve wider window for good operation.

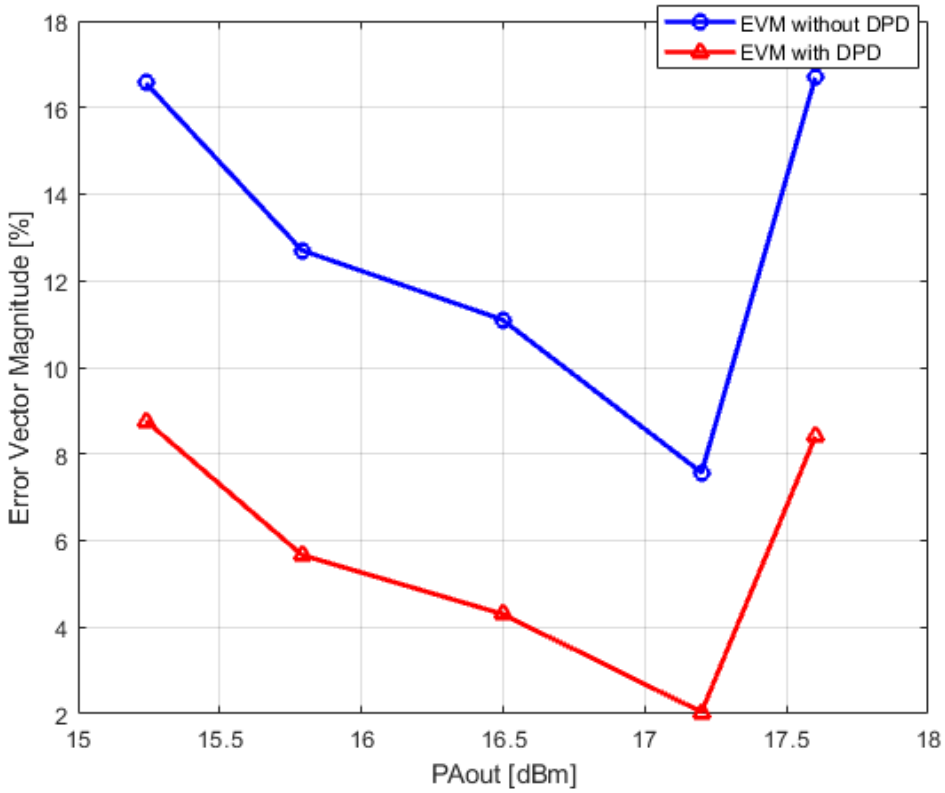

Figure 39. EVM with respect to PA output power with and without DPD.

ACPR as such is a relative measurement and does not always describe the amount of actual interference of the adjacent channels. An ACP measurement helps to radiate limited power into an adjacent channel [48]. In practice, the ACP is interference to other users and systems despite of the channel power level. Hence, ACP can be also measured as absolute power. In the final step, we observe the ACP with respect to output power to measure the nonlinearity of the device. It indicates the amount of spectrum regrowth occurring in the adjacent channel for the existing system. ACP measurement defines the ratio between upper or lower channel powers to main channel power across the bandwidth. Figure 40 shows the ACP with respect to output power with and without DPD.

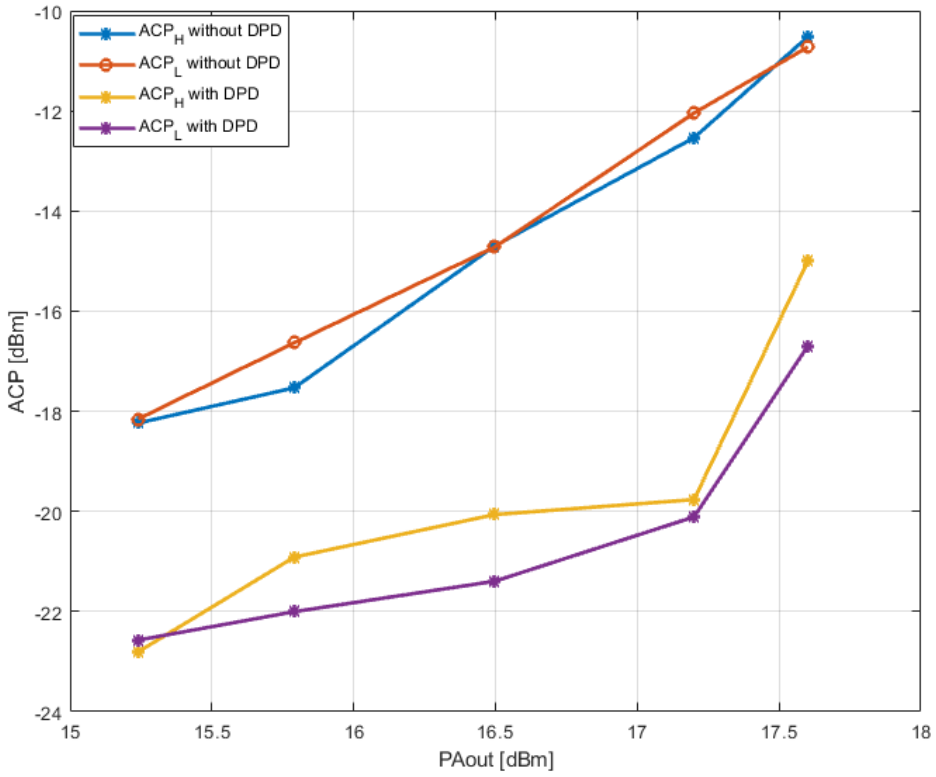

Figure 40. ACP with respect to PA output power with and without DPD.

5. CONCLUSIONS AND FUTURE WORK

This thesis explored the USRP X300 as a demonstration platform for DPD experiments. The USRP radio is a strong and efficient prototyping platform with low cost which is a combination of software and hardware system. By using the SDR platform, we examined the inherent nonlinearity of the PA. For efficient operation, we try to operate the PA in the nonlinear region. Therefore, the nonlinearity increased the out-of-band emissions and also decreased the signal to distortion ratio. In many practical systems, different linearization techniques propose that operate the PA in the saturation region. As a result, signal level is confined in the linear region.

DPD is a common linearization technique where the nonlinearity of the transmit chain is pre-compensated in the digital domain to achieve linear output. Moreover, DPD is used to enable power amplifiers to operate in the power-efficient region with a decent distortion performance. Initially, we calculate the coefficient for characterising the nonlinearity of the PA from the behavioural model. The performance results between the theoretical and simulation are quite different due to the behavioural model is unable to capture the true behaviour of the PA. The reason behind the performance degradation is that the source of nonlinearities and memory effect not only induce from PA but also the ADC and DAC of the USRP daughterboard are also responsible for the total system.

The interfacing between the SIMULINK design and RF measurement setup is another major obstacle. In the SIMULINK model, each sample of the I-Q data is processed on a sample-by-sample basis. However, the I-Q sample from the TX port of the USRP to the external PA and spectrum analyser which capture output signal from the external PA both required hundreds of thousands of samples in a file to be uploaded at a time. This problem can be mitigated by using buffer during transmitting the I-Q data which creates a synchronization problem between the SIMULINK model and the instrumental test bench setup. However, the transmitter and receiver do not follow the frequency and reference time accurately. Therefore, synchronization was required to perform before data decoding correctly. The frequency offset occurs when a difference exists between the transmitter and receiver oscillator frequencies. To avoid such situation we set up the test bench in full duplex mode. The selection of the RF daughterboard is based on the application requirements and also the frequency range. The daughterboard such as CBX and WBX do not have resynchronization feature which resets a fixed offset after each retunes. On the other hand, SBX would be also good for our linearization purpose because of the phased arrays application.

Static, look-up-table based DPD in applied in SIMULINK and the signal is fed through USRP device which acts as a wireless transmitter. The performance of the static LUT-based DPD is evaluated in terms of ACPR and EVM measured at the PA output. To establish a robust SDR platform, MATLAB based simulations using DPD algorithm as well as RF test bench using commercial PA is includes in the RF front end. As we used relatively narrow bandwidth, the memory effects were not present. This indicates that the memory content does not depend on the nonlinearity. By using the DPD in a static model, the ACPR was reduced about 10 dB which remove the out-of-band distortion and also EVM approximately 2.1%. In order to increase the operating region, we have to set the AGC properly. The conclusion to draw from this thesis that USRP might be one good option for demonstrating different algorithm on the real hardware.

During the measurement, only one type of PA behavioural model was used. It would have been interesting to further investigate the DPD with different models and different PA devices. Also, different types of input waveforms could have been studied from single carrier waveforms all the way for OFDM based LTE waveforms. However, this thesis shows that USRP platforms can be used for DPD demonstration. Furthermore, with better control interface such as GNU Radio, the interfacing with USRP would have enabled also adaptive DPD implementation in the FPGA of the USRP itself. Because we selected MATLAB as the control interface, such real-time processing capability was not able to be demonstrated without implementation of new MATLAB interfacing drivers which would have been too vast task for this thesis. The future work will include the demonstration of a DPD system on the real hardware platforms such as ASIC, FPGA and also the complexity study for the different PA behavioural model.

6. REFERENCES

[1] Erdern Bala, Leonid Kazakevich, Rui Yang, "Techniques to Improve Power Amplifier Energy Efficiency for 5G," Inter Digital Communication, Inc., Melville, NY.

[2] https://kb.ettus.com/Synchronization_and_MIMO_Capability_with_USRP_Devices [Access: 20/08/2018]

[3] Smith, A. M., & Cavers, "A wideband architecture for adaptive feedforward linearization," In Vehicular Technology Conference, Vol. 3, pp. 2488-2492, May 1998.

[4] Q. Gu, "RF system design of transceivers for wireless communications". Springer, 2005.

[5] IIari Teikari, "Digital Predistortion Linearization methods for RF Power Amplifiers", Doctoral Dissertation, Helsinki University of Technology, Finland, 2008.

[6] Ahmed Zainudin, Gede Puja Astawa, "Performance Analysis of an OFDM PHY Scheme with Zero Forcing Equalizer using Software Defined Radio Platforms and USRP," EMMITTER International Journal of Engineering Technology, Vol.2, No.1, June 2014.

[7] Aeroflex, "An insight intermodulation distortion measurement methods using the IFR 2026A/B MultiSource Generator," Intermodulation Distortion, Application Note.

[8] Wendy Van Moer, Yves Rolain, Alain Geens, "*Measurement Based Nonlinear Modeling of Spectral Regrowth*", *IEEE MTT-S Digest*, Vol 50, pp. 1711-1716, December 2001.

[9] Dominique Schreurs et al. *RF power amplifier behavioral modeling*. Cambridge University Press New York, NY, USA, 2008.

[10] Rohde & Schwarz, "LTE System Specifications and their impact on RF & Base Band Circuits", Application Note, 1MA221_1E, April 2013.

[11] Michael D. McKinley, Kate A. Remley, Maciej Myslinski2, J. Stevenson Kenney, "EVM Calculation for Broadband Modulated Signals", 64th ARFTG conf. Dig., Orlando, FL, pp.45-52, December 2004.

[12] ElectronicDesign, "Understanding Error Vector Magnitude", Application Note.

[13] S. Boumaiza and F. M. Ghannouchi, "Thermal memory effects modeling and compensation in rf power amplifiers and predistortion linearizers," IEEE Transactions on Microwave Theory and Techniques, vol. 51, Dec 2003.

[14] Gozde Erdogdu, "Linearization of RF Power Amplifiers by using Memory Polynomial Digital Predistortion Technique", Master's Thesis, Middle East Technical University.

[15] Mwangi Stanley Njenga, "Bandwidth Digital Predistortion of Wideband RF Power Amplifiers", Master's Thesis, Tampere University of Technology, Finland.

[16] Yan Ye, Taijun Liu, Tiefeng Xu and Fadhel M. Ghannouchi, *Analysis and Decomposition of the Nonlinearities in RF Power Amplifiers*, *IEEE*, 2010.

[17] Erik Andersson och Christian Olsson, "Linearization of Power Amplifier using Digital Predistortion, Implementation on FPGA", Master's Thesis, Linkopings University, Sweden.

[18] https://kb.ettus.com/About_USRP_Bandwidths_and_Sampling_Rates [Access: 15/03/2018]

[19] Namrata Dwivedi, "Fixed Point Digital Pre-distortion System for Nonlinear High Power Amplifiers," Master's Thesis, IIITD, India.

[20] Mini-Circuits, "Coaxial Amplifier," ZFL-2000+ datasheet.

[21] W. Kester, *The Data Conversion Handbook*, Newnes, 2005.

[22] Jessica Chani Cahuana, "Digital Predistortion for the Linearization of Power amplifiers", Master's Thesis, Chalmers University of Technology, Sweden.

[23] R. N. Braithwaite, "A comparison of indirect learning and closed loop estimators used in digital pre-distortion of power amplifiers," IEEE MTT-S International Microwave Symposium, pp. 1-4, May 2015.

[24] Adaptive DPD Design by Kerry Schutz and Dick Benson, Mathworks.

[25] Morgan, Ma, Kim, Zierdt, Pastalan. "A Generalized Memory Polynomial Model for Digital Pre-distortion of RF Power Amplifiers," IEEE Transactions on Signal Processing, Vol. 54, No. 10, October 2006.

[26] T. Sadeghpour Ghazaany, "Design and Implementation of Adaptive Baseband Pre-distorter for OFDM Nonlineraity Transmiiter", PhD, University of Bradford, England.

[27] Steve C. Cripps, "RF power amplifiers for wireless communications," Artech House microwave library, 1990.

[28] P. Kenington, "High-linearity RF Amplifier Design," Artech House microwave library. Artech House, 2000.

[29] F. M. Ghannouchi, O. Hammi, and M. Helaoui, "Behavioural Modelling and Pre-distortion of Wideband Wireless Transmitters," 1st ed. GB: John Wiley Sons Inc, 2015.

[30] Oualid Hammi and Fadhel M. Ghannouchi, "Power Alignment of Digital Pre-distorter s for Power Amplifiers Linearity Optimization". IEEE Transactions on Broadcasting, 2009.

[31] Matthias Fahale, "Software Defined Radio with GNU Radio and USRP2 Hardware Frontend: Setup and FM/GSM Applications", Bachelor Thesis, Hochschule Ulm, Germany, 2009-2010.

[32] GNU Radio: Tool for exploring the radio frequency spectrum by Eric Blossom on June 1, 2004.

[33] Michael Joseph Leferman, "Rapid Prototyping Interface for Software Defined Radio Experimentation", Master's Thesis, Worcester Polytechnic Institute, United States, 2010.

[34] https://www.edaboard.com/showthread.php?60375-What-does-back-off-in-a-power-amplifier-mean [Access: 30/03/2018]

[35] G. Fettweis, M. Löhning, D. Petrovic, M. Windisch, P. Zillman, and W. Rave, "Dirty RF: a new paradigm," *IEEE Personal Indoor and Mobile Radio Communications*, vol. 4, pp. 2347-2355, September 2005.

[36] Martin Lulf, "Evaluation of Synchronization Algorithm with USRP", Master's Thesis, Technische Universitat Munchen, Germany, 2012.

[37] https://kb.ettus.com/CBX [Access: 01/02/2018]

[38] https://kb.ettus.com/WBX [Access: 01/02/2018]

[39] Mini-Circuits, "Monolithic Amplifier," GVA-84+ datasheet.

[40] Michael Rice. Class Lecture, Topic: “Digital Communications: A Discrete-Time Approach”, Brigham Young University.

[41] https://kb.ettus.com/SBX [Access: 15/02/2018]

[42] Jim Zyren, Al Petrick, “Tutorial Basic Link Budget Analysis”, intersil, June 1998.

[43] Olli Myllari, “Digital transmitter I/O Calibration: Algorithms and Real-Time Prototype Implementation”, Master’s Thesis, Tampere University of Technology, Finland.

[44] https://kb.ettus.com/X300/X310 [Access: 20/01/2018]

[45] Dennis R. Morgan, Zhengxiang Ma, Jaehyeong Kim, “A Generalized Memory Polynomial Model for Digital Pre-distortion of RF Power Amplifiers,” IEEE transactions on Signal Processing, VOL.54, NO.10, October 2006

[46] Cripps, S.C., “A New Technique for Screening and Measuring Channel Temperature in RF and Microwave Hybrid Circuits,” *IEEE Semitherm Symp.,* 1990, pp. 40-42.

[47] https://kb.ettus.com/Selecting_an_RF_Daughterboard [Access: 25/10/2018]

[48] ElectronicDesign, “Understanding Adjacent Channel Power Measurements in Spectrum Analysis”, Application Note.

[49] D.M. Bland, A. Tarczynski, "The effect of sampling jitter in a digitized signal," Proceedings of 1997 IEEE International Symposium on Circuits and Systems, vol. 4, pp. 2685-2688, 1997.

[50] H. Kosugi, T. Matsumoto, T. Uwano, "A High-Efficiency Linear Power Amplifier Using an Envelope Feedback Method", Electronics and Communications in Japan, Part 2, Vol. 77, No. 3, 1994.

[51] H. Paaso and A. Mammela, “Comparison of direct learning and indirect learning predistortion architectures,” in 2008 IEEE International Symposium on Wireless Communication Systems, pp. 309-313, Oct 2008.

[52] R. N. Braithwaite, “A comparison of indirect learning and closed loop estimators used in digital predistortion of power amplifiers,” in 2015 IEEE MTT-S International Microwave Symposium, May 2015, pp. 1-4

[53] D. R. Morgan, Z. Ma, J. Kim, and J. Pastalan, “A generalized memory polynomial model for digital predistortion of RF power amplifiers,” IEEE Trans. Signal Process, vol. 54, no. 10, pp. 3852–3860, Oct. 2006.

[54] R. Raich, “Nonlinear system identification and analysis with applications to power amplifier modeling and power amplifier predistortion,” Ph.D. dissertation, Georgia Institute of Technology, 2004.

[55] Aeroflex, “An insight intermodulation distortion measurement methods using the IFR 2026A/B MultiSource Generator,” Application Note.

[56] Muhammad Yasir Javed, “Characterizing Nonlinearity in Multiantenna Multibeam Transmitters”, Master’s Thesis, University of Oulu, Finland, 2017.

[57] Pedro, José C., Stephen A. Maas. “A comparative overview of microwave and wireless power-amplifier behavioural modeling approaches,” IEEE Transactions on Microwave Theory and Techniques Society, Vol. 53, pp. 1150-1163, April 2005.

[58] F. M. Ghannouchi and O. Hammi, “Behavioral modeling and predistortion,” IEEE Microwave Magazine, vol. 10, no. 7, pp. 52–64, December 2009.

[59] Pedro J.C. & Carvalho N.B. (2002) Intermodulation distortion in microwave and wireless circuits. Artech House.

[60] Joel Vuolevi, T. Rahkonen and Jani Manninen, “Measurement Technique for characterizing memory effects in RF power amplifiers”, *IEEE Radio and Wireless Conference*, August 2002.

[61] ElectronicDesign, “The Difference between Third order Intercept and 1-dB Compression points”, Application Note.

[62] J. Kim and K. Konstantinou, “Digital predistortion of wideband signals based on power amplifier model with memory,” Electronics Letters, vol. 37, no. 23, pp. 1417–1418, Nov 2001.

[63] http://files.ettus.com/manual/page_calibration.html [Access: 02/03/2019]

[64] http://files.ettus.com/manual/page_general.html#general_tuning [Access: 02/03/2019]